universität wien

# MASTERARBEIT

Titel der Masterarbeit

„On the implication of L-type calcium channel-dependent conductances in hippocampal discharge activity“

verfasst von

Manuel Ruiß BSc.

angestrebter akademischer Grad

Master of Science (MSc)

Wien, 2014

| | |
|---|---|
| Studienkennzahl lt. Studienblatt: | A 066 834 |
| Studienrichtung lt. Studienblatt: | Masterstudium Molekulare Biologie |
| Betreut von: | Ao. Univ.-Prof. Dr. Axel Schmid |

This work was carried out at the Department of Neurophysiology and Neuropharmacology (Head: Univ.-Prof. Dr. Stefan Böhm), Center of Physiology and Pharmacology, Medical University of Vienna, under the supervision of Univ.-Lect. Ass.-Prof. Mag. Dr. Helmut Kubista.

# TABLE OF CONTENTS

# 1. INTRODUCTION

## 1.1 Voltage-gated calcium channels (VGCCs)

Voltage-gated ion channels are transmembrane proteins. Besides others, (I) voltage-gated sodium channels (VGSCs), (II) voltage-gated potassium channels (VGKCs), and (III) voltage-gated calcium channels (VGCCs) are important members of this gene superfamily (Ertel et al., 2000; Catterall et al., 2005). As their name already tells, the gating of these proteins is regulated via changes in membrane potential (Vm). In general they open upon membrane depolarization, switch to an inactivated state during persistent depolarization, and close upon hyperpolarization of Vm (Catterall, 2011; Berridge, 2012). Hence, depolarizing signals activate VGCCs leading to calcium-Influx through these channels (Catterall, 2011). Under normal resting conditions ATP-dependent $Ca^{2+}$ pumps on cell surface membranes and on intracellular organelles (e.g. endoplasmic or sarcoplasmic reticulum), as well as a $Na^{+}$-$Ca^{2+}$ exchange system on the cell surface membrane warrant that the concentration of internal free $Ca^{2+}$ ($[Ca^{2+}]_i$) is maintained at low levels (about 0,03 to 0,2 µM) [Hille, 2001]. Calcium-Influx via VGCCs increases $[Ca^{2+}]_i$ and this change in cytoplasmic calcium concentration is recognized by calcium-sensing proteins (e.g. calmodulin, troponin, etc.), which initiate a broad diversity of intracellular events (Hille, 2001; Catterall, 2011). Thus, $Ca^{2+}$ ions can be seen as intracellular second messengers that convert electrical signals of the cell surface to nonelectrical physiological responses in the cell e.g. (I) excitation-transcription coupling, (II) mediation of contraction of cardiac and smooth muscle fibres as well as skeletal muscle cells, (III) initiation of neurotransmitter release, (IV) gating of other ion channels, and (V) regulation of enzyme activity (Ertel et al., 2000; Hille, 2001; Lipscombe et al., 2004; Catterall et al., 2005; Catterall, 2011).

### 1.1.1 Molecular structure of voltage-gated calcium channels

VGCCs are multimeric proteins consisting of a principal $\alpha_1$-subunit and auxiliary subunits. $\alpha_1$ is a large polypeptide (190 to 250 kDa; ~ 2000 amino acid residues), which is organized into four homologous domains (I – IV) interconnected by intracellular loops (Ertel et al., 2000; Hille, 2001; Catterall et al., 2005; Lai and Jan,

2006; Catterall, 2011; Dolphin, 2012). Each of these domains incorporates six alpha-helical transmembrane segments (S1 – S6) with segment 4 forming the arginine rich voltage sensor (Catterall et al., 2005, Lai and Jan, 2006; Catterall, 2011). If a channel is closed, the positive charges of S4 lie within an internal crevice of the $\alpha_1$-subunit. Membrane depolarization then leads to a rotation of the fourth segment and a shift of these arginine residues into an external crevice. This movement of S4 also results in conformational changes of S5 and S6, whereupon the channel pore opens (Cha et al., 1999; Hille, 2001). The fifth and the sixth segment mainly form the pore of the channel and a loop between these segments, which enters the pore from the outside (hence, termed pore loop), acts as an ion selectivity filter of VGCCs (Catterall et al., 2005, Lai and Jan, 2006; Catterall, 2011). Additionally, the $\alpha_1$-subunit contains binding sites for second messengers, drugs, and toxins and therefore accounts for most of the pharmacological properties of VGCCs (Ertel et al., 2000; Hille 2001; Catterall et al., 2005).

The auxiliary subunits consist of a cytosolic β-subunit, which is connected to the $\alpha_1$-subunit via the alpha-interaction domain (AID) on the intracellular loop between domains I and II, and an extracellular $\alpha_2$-subunit that is disulphide-bonded to a membrane associated δ-subunit. A γ-subunit was found in skeletal muscle $Ca^{2+}$ channels, but it remains controversial if it actually is part of neuronal calcium channels (Fig.1). Auxiliary subunits modulate channel properties. Further diversity of calcium channels is achieved through alternative splicing of the $\alpha_1$-subunits (Ertel et al., 2000; Catterall et al., 2005; Catterall, 2011; Berridge, 2012).

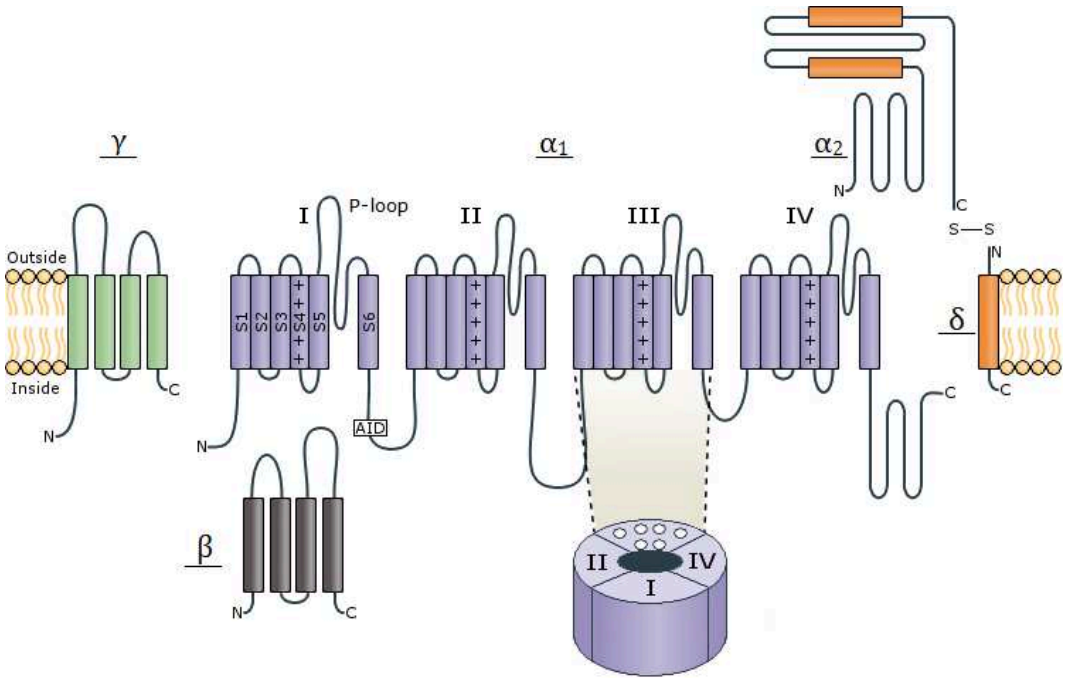

**Figure 1:** Schematic representation of the topology of VGCCs. These channels typically consist of a pore-forming $\alpha_1$-subunit and associated auxiliary β- and α2δ-subunits. The presence of a γ-subunit in neurons has not yet been confirmed. P-loop = pore loop; AID = alpha-interaction domain; + = arginine residues responsible for voltage sensing (modified according to Lai and Jan, 2006; Dolphin, 2009; Catterall, 2011).

### 1.1.2 Terminology and classification of VGCCs

The nomenclature for VGCCs uses the chemical symbol of the permeating ion (Ca) with the main regulator (voltage) as subscript ($Ca_V$). This is followed by the $\alpha_1$-subunit gene subfamily (1 to 3) and the order of its discovery depicted numerically (1 through n). Since there are at least 10 genes encoding for $\alpha_1$-subunits and based on differences in their biophysical and distributional properties, voltage-gated calcium channels can be grouped into three subfamilies (Ertel et al., 2000; Lipscombe et al., 2002; Catterall et al., 2005). $Ca_V1$ channels ($Ca_V1.1$ – $Ca_V1.4$) were termed L-type channels (LTCCs) due to their ability to generate long-lasting $Ca^{2+}$ currents. LTCCs are high-voltage-activated (HVA) because they require strong depolarization for activation. Furthermore, they are sensitive to dihydropyridines (DHP). The $Ca_V2$ family is also HVA, but unlike $Ca_V1$, is not affected by DHPs (Ertel et al., 2000; Catterall et al., 2005; Catterall, 2011; Berridge, 2012). $Ca_V2.2$ was the first member of $Ca_V2$ calcium channels, which was discovered. This isoform was primarily described in chick sensory neurons and showed single-channel conductances intermediate between those of the T- and L-types. Thus, it was termed N-type channel (“neither T nor L” or “neuronal”; NTCC) [Nowycky et al., 1985b; Fox et al., 1987]. NTCCs were further subdivided with the help of snail toxins (Hille, 2001). $Ca_V2.2$ was sensitive to ω-Conotoxin, whereas another isoform, $Ca_V2.1$, was affected by ω-Agatoxin. $Ca_V2.1$ was termed P/Q-channel (PTCC/ QTCC), with P standing for Purkinje cells of the cerebellum, where they first were discovered (Llinás et al., 1989; Hille, 2001; Catterall, 2011). $Ca_V2.3$ was resistant to these toxins and, hence, was named R-type channel (RTCC) [Hille, 2001; Catterall, 2011]. In contrast the $Ca_V3$ family of T-type channels ($Ca_V3.1$ – $Ca_V3.3$; TTCCs), so called because of their transient calcium currents, can be considered as low-voltage-activated (LVA) because they respond to smaller membrane potential changes (Table 1) [Ertel et al., 2000; Catterall et al., 2005; Catterall, 2011, Berridge, 2012].

| Channel | Type | Pharmacology | Tissue distribution | |
|---|---|---|---|---|
| $Ca_V1.1$ ($\alpha_{1S}$) | L-type | Dihydropyridines | Skeletal muscle | HVA |
| $Ca_V1.2$ ($\alpha_{1C}$) | | | Heart, CNS, endocrine cells | |
| $Ca_V1.3$ ($\alpha_{1D}$) | | | Heart, CNS, endocrine cells | |
| $Ca_V1.4$ ($\alpha_{1F}$) | | | Retina | |
| $Ca_V2.1$ ($\alpha_{1A}$) | P/Q-type | ω-Agatoxin | CNS, neuromuscular junction | HVA |
| $Ca_V2.2$ ($\alpha_{1B}$) | N-type | ω-Conotoxin | | |
| $Ca_V2.3$ ($\alpha_{1E}$) | R-type | SNX-482 | | |
| $Ca_V3.1$ ($\alpha_{1G}$) | | Kurotoxin | CNS, heart, smooth muscle | |
| $Ca_V3.2$ ($\alpha_{1H}$) | T-type | Kurotoxin, Mibefradil | CNS, heart, liver, kidney | LVA |
| $Ca_V3.3$ ($\alpha_{1I}$) | | | CNS | |

**Table 1:** Classification of VGCCs. Overview of the functional and pharmacological properties, the location throughout the body, and the activation modalities of the different isoforms of voltage-gated calcium channels. Genes encoding for the respective $\alpha_1$-subunit are shown in parenthesis (modified according to Catterall et al., 2005; Catterall, 2011; Berridge, 2012).

### 1.2 L-type voltage-gated calcium channels (LTCCs)

Although the four isoforms ($Ca_V1.1$ to $Ca_V1.4$) of the $Ca_V1$ gene family share some common features, they also exhibit differences in several properties for example in their distribution and their function.

#### 1.2.1 Electrophysiological characteristics of the $Ca_V1$ gene family

Generally speaking LTCCs open upon strong depolarization (beyond approximately -30 mV) and are therefore referred to as high-voltage-activated channels (Lipscombe et al., 2004; Alexander et al., 2011). However, transient expression experiments showed that activation of $Ca_V1.3$ takes place at more hyperpolarized potentials (-45,7 mV ± 0,5 mV) compared to that of $Ca_V1.2$ (-31,5 mV ± 0,5 mV) [Koschak et al., 2001]. These findings are in accordance with a report in which it was found that the first isoform opened at approximately -55 mV, whereas currents of the latter isoform could be evoked by depolarization to at least -35 mV (Xu and Lipscombe, 2001). Together these data suggest that $Ca_V1.3$ activates at membrane potentials which are -15 mV to -25 mV more hyperpolarized compared to $Ca_V1.2$. Hence, the $Ca_v1.3$ isoform can be considered medium-voltage-activated (MVA). However, in a parallel study of our group, in which current injection experiments were carried out in primary $Ca_V1.3^{-/-}$ mice hippocampal neurons, it was found that $Ca_V1.2$ operates over a broad voltage range (-48 mV to -35mV). Thus, their function may also not be limited to high membrane voltages (Hasreiter, 2012).

Furthermore LTCCs have slow inactivation kinetics, meaning that they remain responsive to maintained depolarization, which is important to control physiological processes (e.g. muscle contraction, hormone secretion, and gene activation), where $Ca^{2+}$ is required for longer time periods (Koschak et al., 2001; Lipscombe et al., 2004; Alexander et al., 2011; Berridge, 2012). Inactivation, in most cases, is calcium-dependent, except for the $Ca_V1.4$ isoform, which is not inactivated in a calcium-dependent manner (Alexander et al., 2011; Baumann et al., 2004; Lipscombe et al., 2004; McRory et al., 2004). Additionally, all of the members of the $Ca_V1$ subfamily exhibit a high single-channel conductance (Lipscombe et al., 2004; Berridge, 2012).

### 1.2.2 Distribution and function of individual LTCC isoforms

1.2.2.1 $Ca_V1.1$ ($\alpha_{1S}$): The $Ca_V1.1$ isoform of LTCCs is primarily expressed in the transverse tubules of skeletal muscle, where it is connected to the type 1 ryanodine-sensitive $Ca^{2+}$ release channel (RyR1) in the sarcoplasmatic reticulum (Flucher and Franzini-Armstrong, 1996; Lipscombe et al., 2004; Catterall et al., 2005; Calin-Jageman and Lee, 2008; Berridge, 2012). $\alpha_{1S}$ acts more as a voltage sensor, which couples depolarization to RyR1 activation, than as a $Ca^{2+}$-Influx channel (Lipscombe et al., 2004).

1.2.2.2 $Ca_V1.2$ ($\alpha_{1C}$) and $Ca_V1.3$ ($\alpha_{1D}$): $Ca_V1.2$ and $Ca_V1.3$ can be found in neuroendocrine cells, pancreatic cells, and neurons. $\alpha_{1C}$ is additionally expressed in smooth muscle, fibroblasts, and ventricular cardiac muscle and is suggested to play a functional role in long term potentiation and spatial memory, regulation of gene expression, hormone secretion, and excitation-contraction coupling in cardiac and smooth muscles. $\alpha_{1D}$ is further located in sensory cells of the inner ear and contributes to pacemaking in cardiac atrial myocytes (Clark et al., 2003; Lipscombe et al., 2004; Catterall et al., 2005; Moosmang et al., 2005; Calin-Jageman and Lee, 2008; Catterall, 2011; Berridge, 2012). Both isoforms are the main fraction of LTCCs in the brain, with $Ca_V1.2$ predominating (80%) over $Ca_V1.3$ (20%) [Clark et al., 2003; Trimmer and Rhodes, 2004; Calin-Jageman and Lee, 2008; Lacinova et al., 2008].
In neurons $Ca_V1.2$ is mainly localized to the soma and to dendrites and dendritic spines. However, a small portion of this isoform can also be found in axons and axonal terminals. $Ca_V1.3$ is found a little bit more distal in the vicinity of axosomatic

and axodendritic synapses at dendritic spines (Trimmer and Rhodes, 2004; Catterall et al., 2005; Calin-Jageman and Lee, 2008; Tippens et al., 2008; Dolphin, 2012). In situ hybridization (ISH) experiments with specific ribopropes for $\alpha_1$-subunit ($\alpha_{1A}$, $\alpha_{1B}$, $\alpha_{1C}$, and $\alpha_{1D}$) mRNA showed that $\alpha_{1C}$ and $\alpha_{1D}$ are predominantly expressed in olfactory bulb, hippocampus, and cerebellum. However, throughout the hippocampus $Ca_V1.2$ was only found in moderate amounts in the dentate gyrus (DG), whereas $Ca_V1.3$ showed a strong distribution in DG (Ludwig et al., 1997). In accordance to these findings, ISH experiments revealed that $\alpha_{1D}$ mRNA is expressed in all regions of the hippocampus, but predominantly in DG in young rats, whereas their expression increases in cornu ammonis region 1 (CA1) in older rats (Herman et al., 1998).

1.2.2.3 $Ca_V1.4$ ($\alpha_{1F}$): The $Ca_V1.4$ isoform is mainly found in the retina, where it is located at the synaptic terminal between rod photoreceptors and bipolar cells (Lipscombe et al., 2004; Calin-Jageman and Lee, 2008). Furthermore, this channel is expressed in dorsal root ganglia of the spinal cord and in lymphoid tissue (plasma cells and mast cells) [Lipscombe et al., 2004; Catterall et al., 2005]. Its most important function is the release of glutamate from photoreceptors in the dark, which is crucial for responding to visual stimuli (Catterall et al., 2005; Calin-Jageman and Lee, 2008).

### 1.2.3 Pharmacological properties of LTCCs

L-type voltage-gated $Ca^{2+}$ channels can be inhibited reversibly by three classes of drugs: dihydropyridines (DHP), phenylalkylamines (PAA), and benzothiazepines (BTZ) (Fig.2) [Hille, 2001; Kochegarov, 2003; Elmslie, 2004; Catterall, 2011].

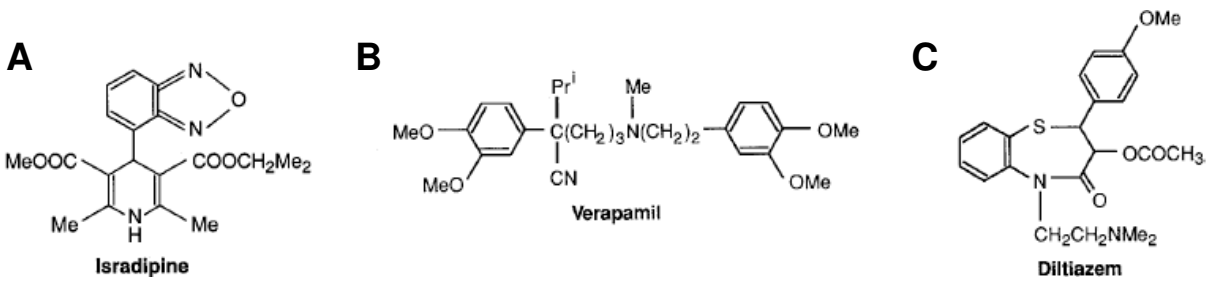


**Figure 2:** Structure of the major compounds of the three classes of LTCC antagonists (A. dihydropyridines, B. phenylalkylamines, C. benzothiazepines) [modified according to Triggle, 2003].

Dihydropyridines typically contain one pyridine ring and one benzene cycle (Fig.2A). They can either decrease $Ca^{2+}$ current (antagonists like isradipine, nifedipine or nimodipine) or increase it (agonist, Bay K 8644). LTCCs show three different gating modes: mode 0 represents a closed state, mode 1 describes short channel openings (~ 1 ms), and mode 2 stands for long channel openings (> 10 ms). Contrary to PAAs and BTZs, DHP antagonists work in a "state-dependent" manner, meaning that they preferentially bind to channels which are depolarized for some time and therefore become inactivated. Via this mechanism DHP antagonists, like isradipine, bind and stabilize this inactivated conformation (mode 0). Hyperpolarizations, which favour recovery from the inactivated state, promote unbinding of DHP antagonists. In contrast, the DHP agonist enantiomer (-)-(S)-Bay K 8644 (BayK), stabilizes long channel openings (mode 2 gating) (Nowycky et al., 1985a; Hille, 2001; Kochegarov, 2003; Elmslie, 2004; Catterall et al., 2005; Alexander et al., 2011). However, 5 µm nifedipine, a dihydropyridine LTCC antagonist, inhibited the current through the $Ca_V1.2$ channel completely within 12 seconds, whereas 20% of $Ca_V1.3$ current remained after 20 seconds exposure to this antagonist (Helton et al., 2005). Furthermore, $Ca_V1.3$ showed a 20-fold lower sensitivity to the DHP-blocker nimodipine compared to $Ca_V1.2$, whereas isradipine, an antagonist of the same class of drugs, exhibited a 8,5-fold higher potency for $Ca_V1.2$ than for $Ca_V1.3$ (Koschak et al., 2001; Xu and Lipscombe, 2001). $Ca_V1.4$ has only moderate sensitivity against diltiazem, which is an antagonist of the benzothiazepine class. Additionally, sensitivity of this isoform to isradipine was approximately 20-fold lower than for $Ca_V1.2$ (Baumann et al., 2004).

A major compound of the phenylalkylamine group is verapamil. It consists of two benzene cycles that are connected to a nitrogen atom via carbohydrate chains (Fig.2B). PAAs are considered „use-dependent"-pore blockers, meaning that the inhibiting effect of this class of antagonists increases with repetitive stimulation of $Ca^{2+}$ channels. PAAs enter the channel from the cytoplasmatic site when the pore is open and they keep the channel in an inactive conformation, which makes further binding of PAAs easier. The probability of $Ca^{2+}$ channel inhibition increases with repetitive open-inactivated cycles of the channel.

Diltiazem, a typical member of the benzothiazepine class, contains two benzene cycles connected via nitrogen and sulphur atoms (Fig.2C). This family of drugs

enters the pore from the extracellular side and, as PAAs, they act as pore blockers (Hille, 2001; Kochegarov, 2003; Elmslie, 2004; Catterall et al., 2005).
Each of the drugs described above act at different sites on the $\alpha_1$ subunit (Hille, 2001; Elmslie, 2004; Catterall et al., 2005). PAAs and BTZs bind to amino acid residues in the S6 segment of domains III and IV, whereas dihydropyridines additionally bind the S5 segment of domain III. However, their binding sites overlap in the S6 segments of the LTCCs (Kochegarov, 2003; Elmslie, 2004; Catterall et al., 2005).
$Ca^{2+}$ antagonists are used in the treatment of diseases like hypertension, arrhythmia, angina pectoris, and congestive heart failure. Furthermore, some DHPs were patented for treatment of neuronal disorders like Alzheimer's disease, Parkinson's disease, or migraine (Kochegarov, 2003; Elmslie, 2004).

### 1.3 The role of LTCCs in neuronal excitability

LTCCs play a crucial role in the regulation of neuronal excitability and this is primarily due to the coupling of LTCC-mediated $Ca^{2+}$-Influx to $Ca^{2+}$-dependent conductances.

#### 1.3.1 The implication of LTCCs in generation of after-potentials

The current clamp mode in patch clamp experiments offers the possibility to depolarize, by the use of current injections, a neuron to the membrane potential at which LTCCs become activated. Thereby a voltage response, that starts and ends simultaneously with this current pulse, is evoked. However, in some neurons the membrane potential does not immediately return to the baseline membrane potential when the current injection is turned off, but instead elicits a so called after-potential upon application of BayK. Such after-events can be subdivided into after-depolarizations (ADPs) or after-hyperpolarizations (AHPs).
In a previous study of our group current injections were employed in the presence of tetrodotoxin [TTX, a blocker of voltage-gated $Na^+$ channels and therefore action potentials] to study these events in primary rat hippocampal neurons in more detail. It was shown that ADPs (Fig.3A1) as well as AHPs (Fig.3A2) were elicited in some neurons already under control conditions (DMSO), were potentiated in the presence of the LTCC agonist BayK, but were reduced or completely absent when the LTCC

antagonist isradipine was applied (Geier et al., 2011). In the same set of experiments, blockade of nonspecific cation channels (CANs) via flufenemic acid (FFA) reduced LTCC-mediated current injection-induced after-depolarizations (Geier et al., 2011). Similar results were observed in slices of substantia nigra pars reticulate GABAergic neurons and in slices of the dentate gyrus (Lee and Tepper, 2007; Hofmann and Frazier, 2010) [Fig.3B]. Together these results show that after-depolarizations are mediated via LTCC-mediated CAN activation. However, CAN currents ($I_{CAN}$) have only been described in electrophysiological terms and their molecular identity remains unclear. According to the literature two members of the melastatin-related subfamily of transient receptor potential channels (TRPM) seem to be the most promising candidates underlying ADP-generation (Launay et al., 2002; Hofmann et al., 2003; Nilius et al., 2005; Ullrich et al., 2005; Teruyama and Armstrong, 2007; Smith and Araneda, 2010). These are TRPM4b and TRPM5, which exhibit unique features within the TRP superfamily (Ullrich et al., 2005; Teruyama and Armstrong, 2007). Both of these channels are permeable for monovalent cations ($Na^+$ and $K^+$), whereas they are impermeable to $Ca^{2+}$. Furthermore, TRPM4b and TRPM5 can be activated by calcium and they are sensitive to blockade by FFA (Hofmann et al., 2003; Nilius et al., 2005; Ullrich et al., 2005; Teruyama and Armstrong, 2007). However, since selective antagonists for both of these subtypes of the TRP channel family are lacking, the molecular identity of the channels underlying CAN currents still remains elusive (Teruyama and Armstrong, 2007; Mrejeru et al., 2011). Additionally, it was found in a previous study of our group that after-depolarizations are completely missing in hippocampal neurons of $Ca_V1.2$ mice, which exhibit decreased sensitivity for dihydropyridines due to a pharmacological knockout ($Ca_V1.2$ $DHP^{-/-}$). Hence, ADPs seem to be mediated solely via $Ca_V1.2$ (Goldnagl, 2012).

In contrast, AHPs following a current injection can be subdivided into a fast (fAHP), a medium (mAHP), and a slow (sAHP) component (Fig.3C). As the nomenclature already tells fast after-hyperpolarizations can be detected immediately (1 – 5 ms) after individual action potentials. Its underlying current is $Ca^{2+}$- and voltage-dependent and can be inhibited by blockers of BK (big conductance)-type potassium channels (Gamelli et al., 2011; Andrade et al., 2012). Contrary, medium AHPs appear with a decay of about 100 ms after current injections. They are supposed to be generated by an apamin-sensitive, calcium-activated potassium channel, namely

a SK (small conductance, $K_{Ca}2.x$)-type channel (Gamelli et al., 2011; Andrade et al., 2012). However, in another study apamin, a $K_{Ca}2.x$ inhibitor, failed to block the mAHP in rat CA1 pyramidal cells (Gu et al., 2005). Slow after-hyperpolarizations usually occur after about 1 – 5 seconds. The current underlying the sAHP is calcium-dependent and knockout of the LTCC $Ca_V1.3$ isoform in mouse CA1 pyramidal neurons reduced the area of the sAHP, but it was not affected by deletion of the gene encoding the $Ca_V1.2$ isoform (Gamelli et al., 2011). Furthermore, slow after-hyperpolarizations are strongly affected by different neuromodulators (Gamelli et al., 2011; Andrade et al., 2012). Recent studies suggested that there might be an intermediate step between activation of calcium-dependent potassium channels via $Ca^{2+}$-Influx through LTCCs and generation of the sAHP. For example it was suggested that calcium may increase the expression of membrane phosphatidylinositol 4,5-biphosphate [$PtdIns(4,5)P_2$], which controls multiple potassium channels, in the vicinity of channels underlying slow after-hyperpolarizations. Therefore, activation of potassium channels via $Ca^{2+}$-dependent increase in $PtdIns(4,5)P_2$ could be the underlying mechanism of sAHPs (Andrade et al., 2012).

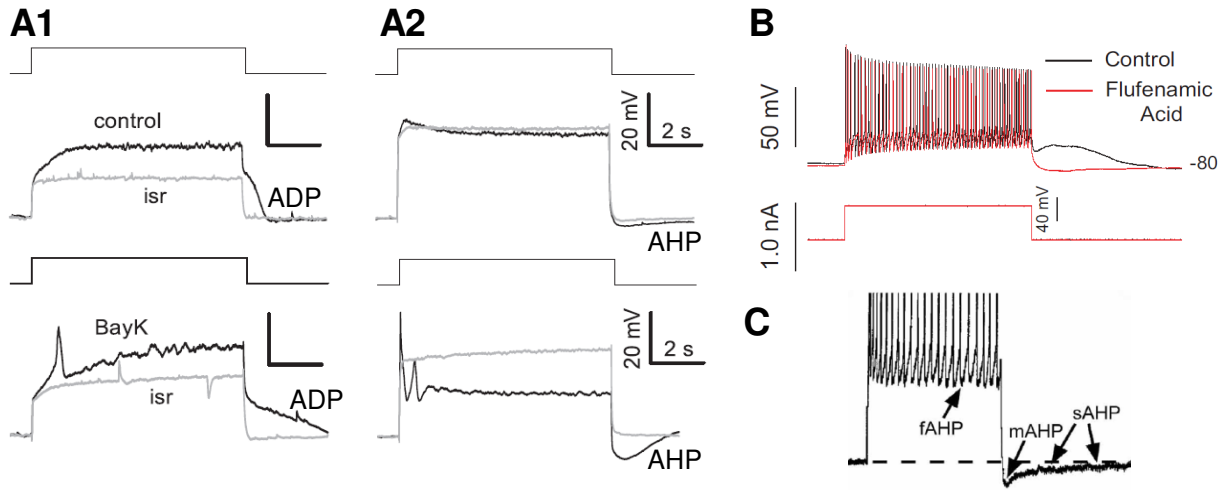


**Figure 3:** Current injection experiments to evoke and to study after-potentials. A. After-depolarizations (ADP; A1) and after-hyperpolarizations (AHP; A2) were evoked by current injections in the presence of tetrodotoxin (TTX) and DMSO (control; black upper traces). Application of the LTCC agonist Bay K 8644 (BayK) led to potentiation of both after-potentials (black lower traces), whereas the LTCC blocker isradipine (isr; grey traces) eradicated both after-potentials. B. Use of flufenemic acid (FFA), an inhibitor of calcium-dependent nonselective cation conductances ($I_{CAN}$), abolished the ADP compared to control conditions. C. Trains of action potentials evoked by current injections are followed by a medium and a slower AHP, whereas the fast AHP occurs directly after a single action potential (modified according to Geier et al., 2011 [A], Lee and Tepper, 2007 [B] and Andrade et al., 2012 [C]).

### 1.3.2 LTCC-mediated active voltage responses

In the same experiments as described in subchapter 1.3.1 our group found out that current injections in the presence of the LTCC agonist are able to give rise to 3 different types of active voltage responses. One of them was – according to its general appearance – termed “bump” and describes a sustained depolarization in the presence of BayK, which is absent in traces recorded with isradipine (Fig.4A1). In contrast, “hyperpolarizing sag” denotes a situation in which the LTCC agonist elicits more hyperpolarized voltage responses than those seen in measurements done under application of the LTCC antagonist (Fig.4A3). Finally, in the presence of BayK, oscillatory voltage changes, termed “oscillations”, could be detected in some neurons (Fig.4A2). Interestingly, ADPs were correlated with bumps and both were evoked at milder depolarization levels, whereas AHPs and hyperpolarizing sags could be elicited upon stronger stimulation. However, no correlation between oscillations and one of these after-potentials could be detected (Geier et al., 2011).

A partial reduction of bumps occurred when FFA was applied, suggesting that CAN channels are involved. In contrast hyperpolarizing sags were augmented in the presence of apamin, indicating that these active voltage responses are evoked largely due to activation of $K_{Ca}2.x$ channels (Geier et al., 2011).

Summarized these findings indicate that upon current injection, some neurons react with a bump and an ADP, mediated via coupling of $Ca^{2+}$-Influx of LTCCs to $I_{CAN}$ (excitatory coupling), whereas others are prone to generation of hyperpolarizing sags and AHPs, mediated via coupling of $Ca^{2+}$-Influx of LTCCs to calcium-dependent $K^+$-conductance ($K_{Ca}$) [inhibitory coupling] (Fig.4).

**Figure 4:** Summary of the mechanisms involved in the generation of after-potentials and LTCC-mediated voltage responses. $Ca^{2+}$-Influx via L-type voltage-gated $Ca^{2+}$ channels leads to activation of nonspecific cation channels (CAN; B1) giving rise to after-depolarizations (ADP) and bumps (excitatory coupling; A1). Contrary, coupling of LTCCs to calcium-dependent $K^+$-channels ($K_{Ca}$; probably SK channels; B2) is involved in the generation of after-hyperpolarizations (AHP) and hyperpolarizing sags (inhibitory coupling; A3). However, oscillations represent an intermediate response type, which seems not to be correlated with any of these after-potentials (A2). A1 – A3 were taken from and modified according to Geier et al., 2011.

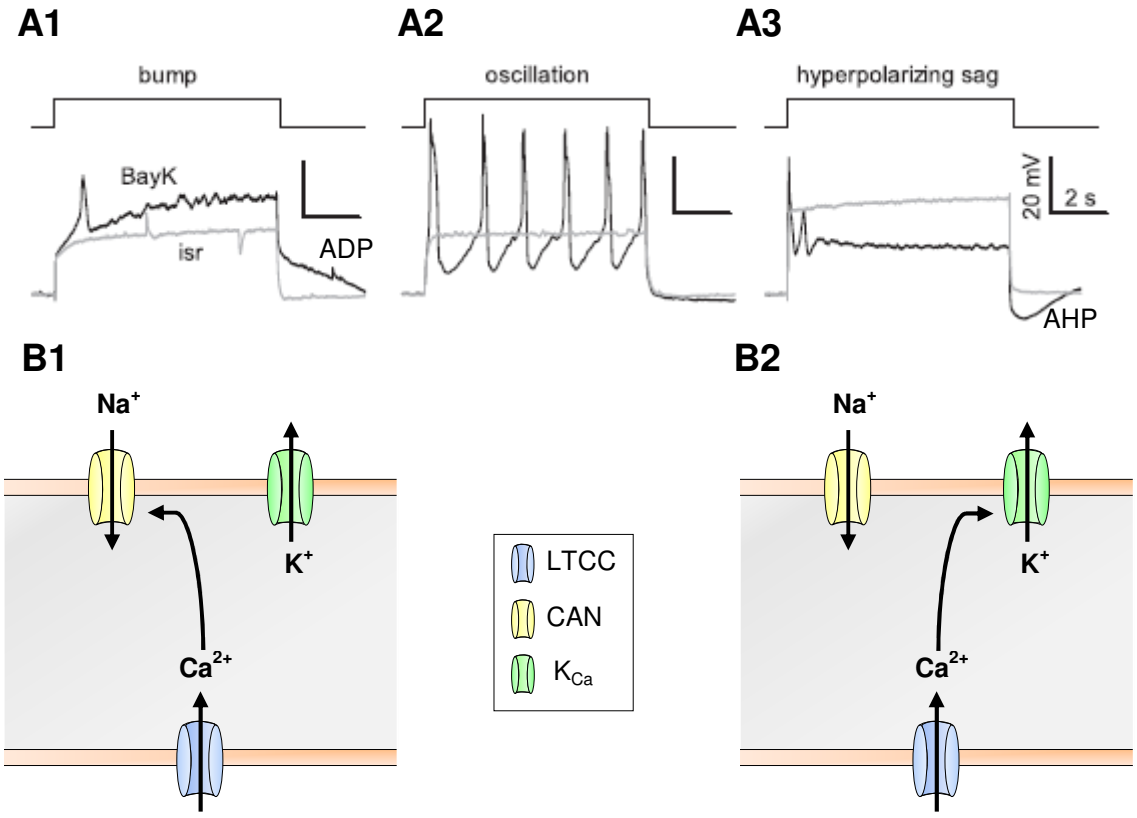


### 1.3.3 Implication of after-potentials in neuronal electrical activity

Bursts are defined as brief trains of high-frequency action potentials, which ride on top of a depolarization wave. These discharge patterns are intrinsic properties of a subpopulation of neurons in different brain areas (e.g. septum, reticular formation, inferior olive, CA1 to CA3 of the hippocampus, etc.) [Lisman, 1997; Perez-Reyes, 2003; Bean, 2007; Kim and Trussell, 2007].

Bursts are supposed to be network-driven via synaptic inputs or intrinsically evoked via low threshold calcium spikes (LTS) [Lisman, 1997; Overton and Clark, 1997; Beurrier et al., 1999; Perez-Reyes, 2003]. Both mechanisms lead to a depolarization that gives rise to L-type $Ca^{2+}$ currents ($I_L$), which initiate the plateau phase of the burst. Additionally, $Na_v$ and $K_v$ channels, which are involved in the generation and the repolarization of sodium spikes, respectively, become activated. In turn, these $Na^+$ spikes increase $Ca^{2+}$-Influx through LTCCs, and probably other HVA $Ca^{2+}$ channels. This increase in internal calcium concentration then gives rise to $Ca^{2+}$-dependent $K^+$ currents ($I_{K,Ca}$) leading to a gradual decline of the plateau (Beurrier et al., 1999; Perez-Reyes, 2003). Furthermore, it was hypothesized in the literature that nonspecific cation channel current ($I_{CAN}$) may contribute to initiation and/ or

prolongation of the burst plateau phase (Fig.5) [Beurrier et al., 1999; Pape et al., 2004; Lee and Tepper, 2007].

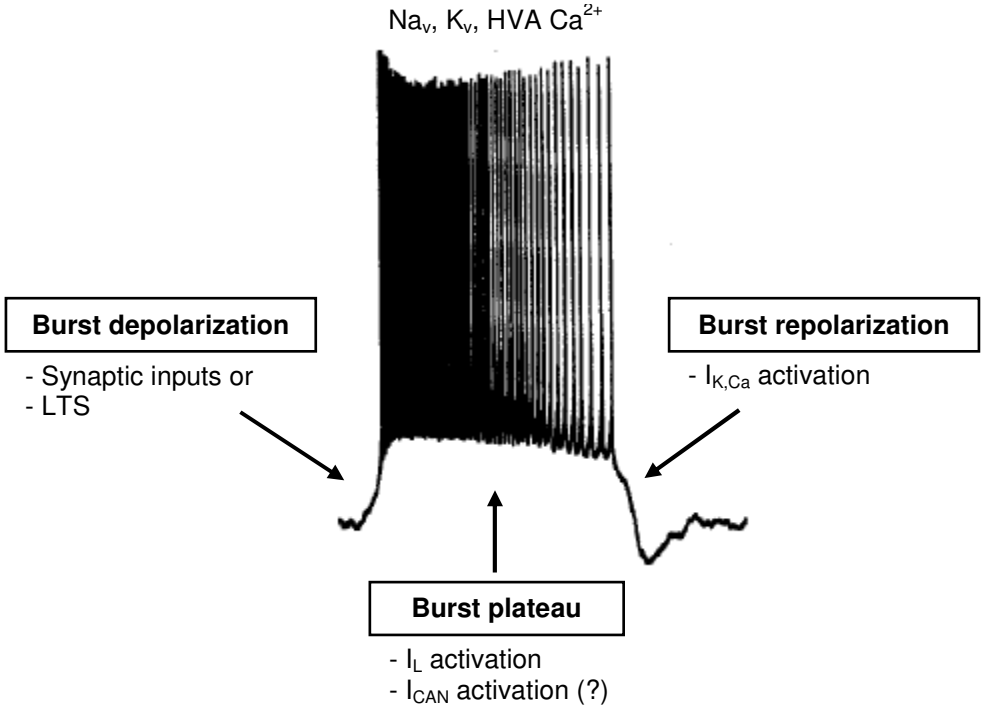


**Figure 5:** Currents underlying burst firing. An initial depolarisation (via synaptic inputs or low threshold calcium spikes) leads to sodium-dependent spikes evoked via voltage-gated $Na^+$ channels. L-type $Ca^{2+}$ currents ($I_L$), and probably nonspecific cation currents ($I_{CAN}$), participate in the initiation and maintenance of the burst plateau. Activation of $Ca^{2+}$-dependent $K^+$ currents ($I_{K,CA}$) then leads to a decline of the membrane potential (modified according to Beurrier et al., 1999).

In experiments using current injections to evoke action potentials followed by an after-depolarization it was found that such after-potentials, when they exceed the spike threshold, can give rise to a second or more action potentials. Hence, it was suggested that large ADPs are able to convert tonic firing into a bursting firing mode (Bean, 2007; Beck and Yaari, 2008; Brown and Randall, 2009) [Fig.6A]. This hypothesis was further analysed by application of flufenemic acid to dopaminergic neurons of the substantia nigra pars compacta which fired in burst mode. After five to ten minutes in the bath, FFA terminated bursting in these cells and gave rise to tonic firing. This process was reversible (Mrejeru et al., 2011) [Fig.6B]. In contrast potentiation of SK channels via application of 1-EBIO promoted conversion of burst firing into a single-spike pattern, whereas inhibition of these channels with apamin reversed this effect (Cingolani et al., 2002; Liu and Herbison, 2008; Chen and Toney,

2009) [Fig.6C]. According to these results after-depolarizations may function as a trigger of excitation, whereas after-hyperpolarizations counteract this situation.

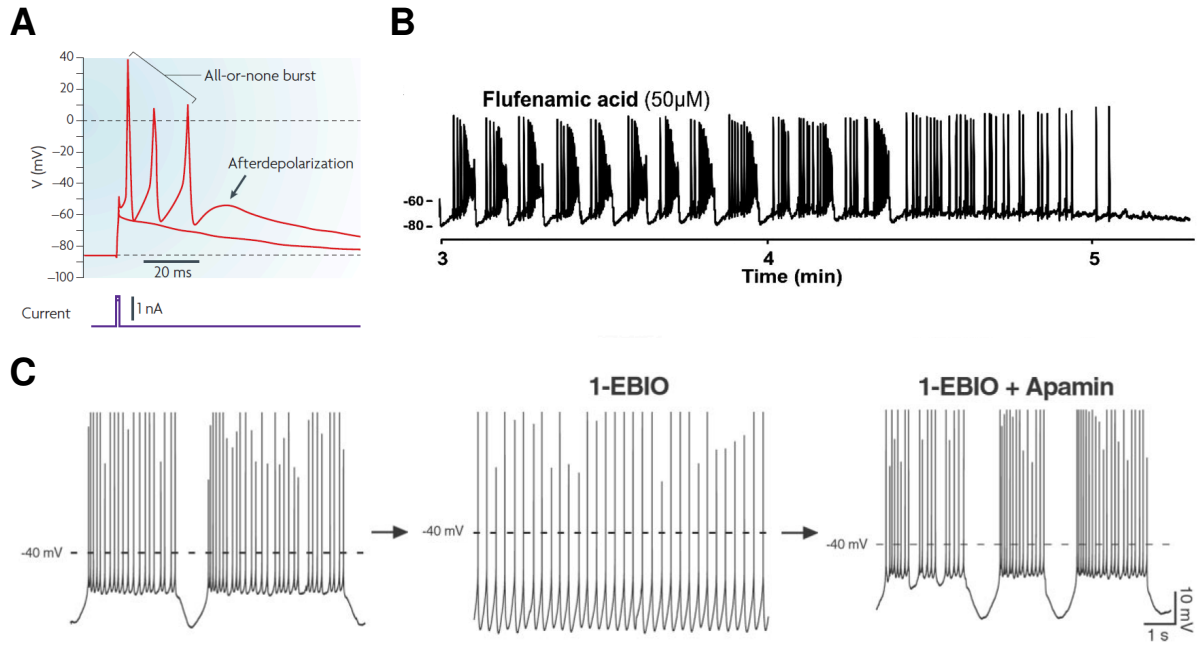


**Figure 6:** Involvement of after-potentials in neuronal excitability. A. After-depolarizations that reach threshold levels can enhance a single action potential leading to burst firing. B. This discharge pattern can be abolished by blockade of the nonspecific cation current ($I_{CAN}$) via flufenemic acid (FFA). C. In contrast, a SK channel enhancer (1-EBIO), converts bursting into tonic firing, a condition that is reversed during application of the SK channel blocker apamin [modified according to Bean, 2007 (A), Mrejeru et al., 2011 (B), and Cingolani et al., 2002 (C)].

### 1.3.4 Implication of excitatory and inhibitory coupling in physiological and pathological conditions

To test if neuronal intrinsic excitability is involved in the cellular substrates underlying learning and memory, Disterhoft and colleagues, carried out eyeblink conditioning experiments in rabbits. Therefore, a conditioned stimulus (CS, flashlight) was paired with an unconditioned stimulus (US, airpuff to the eye) to yield closure of the eyelid. Association of both stimuli was achieved after several repetitions leading to a situation in which the CS alone was able to evoke eyeblinking. In electrophysiological recordings it was shown afterwards that in CA1 hippocampal neurons of rabbits, which had learned the task, neuronal excitability was increased and that the post-burst AHP had become smaller as compared to cells from the control group. Furthermore, magnitude of the AHP was dependent on the learning success, meaning that rabbits who learned the task well showed smaller AHPs. These results

were confirmed in learning experiments using the spatial water-maze task (Disterhoft and Oh, 2006).

Furthermore, other studies demonstrated that AHPs were increased in size in aged rats as compared to the situation in younger ones and this was taken as a possible explanation for learning impairments in aging individuals (Landfield and Pitler, 1984; Kumar and Foster, 2002; Moyer et al., 2002; Power et al., 2002). This increase in the magnitude of the after-hyperpolarization was suggested to be due to an increase in L-type voltage-gated calcium channel expression and/ or distribution in the aging brain leading to changes in neuronal activity (Brewer et al., 2009; Núñez-Santana et al., 2014).

Additionally it was suggested, that firing mode changes are involved in neurodegenerative diseases. For example, the muscarinic agonist pilocarpine can be used to induce status epilepticus, in which initial seizures are evoked. After these epileptic signs come to an end a latent phase occurs in which the animals behave normally. This is followed by spontaneous unprovoked seizures and structural as well as functional changes, which are comparable to those seen in human temporal-lobe epilepsy (Beck and Yaari, 2008). In hippocampal CA1 pyramidal or subicular neurons of animals treated with pilocarpine, tonic firing was converted into a bursting mode followed by a spike after-depolarization (Zhang and Linden, 2003). Another hint for the involvement of changes in intrinsic excitability in the generation of epilepsy comes from the kindling model in which mAHP and sAHP seem to be downregulated (Beck and Yaari, 2008).

### 1.4 Aim of the study

Hippocampal neurons can be distinguished with respect to their preferential coupling to CANs or $K_{Ca}$s and these $Ca^{2+}$-dependent conductances are suggested to play a crucial role in neuronal excitability. To shed light on this role, I tested for functional links between the preferential LTCC coupling and the predominant neuronal activity.

# 2. MATERIAL AND METHODS

## 2.1 Primary cell culture of rat hippocampal neurons

Neonatal Sprague-Dawley rats were killed by decapitation according to the rules of the Austrian animal protection law (see https://www.ris.bka.gv.at/GeltendeFassung.wxe?Abfrage=Bundesnormen&Gesetzesnummer=20003541) and the Austrian animal experiment by-laws (see http://www.ris2.bka.gv.at/Dokumente/BgblPdf/2000_198_2/2000_198_2.pdf). After opening of the cranium, the brains were placed in a culture dish filled with 2 ml autoclaved and sterile-filtered, ice-cold PUCK-KYN-solution. This buffer contained 137 mM NaCl, 4,5 mM KCl, 1,1 mM $Na_2HPO_4$ x 2 $H_2O$, 1,1 mM $KH_2PO_4$, 6,1 mM glucose, and 1 mM kynurenate (NMDA receptor antagonist). The solution then was adjusted to pH 7,3 with NaOH. All ingredients were purchased from Sigma-Aldrich (Vienna, Austria).

By using a stereo microscope, the two cerebral hemispheres were detached from each other, separated from the meninges, and positioned with the inner surface pointing upwards, allowing easy identification of the hippocampi in the middle of each brain half. After removing them with a scalpel and sharp scissors, they were placed in a separate culture dish containing ice-cold PUCK-KYN solution, wherein the remaining parts of connective tissue and blood vessels were removed. Before transferring the hippocampi in papain solution (25 units/ ml; Worthington, Lakewood, U.S.A.), hippocampi were incised with a scalpel for better invasion of the enzyme and then they were incubated for about 15 minutes at 37°C (5 % $CO_2$).

The following steps were carried out in a laminar-flow hood under sterile conditions. To terminate enzymatic digestion, hippocampal pieces were placed into ice-cold stop solution (PUCK-KYN-solution with 25% heat inactivated fetal calf serum [FCS]; Invitrogen, Lofer, Austria). Then they were transferred in D-MEM medium containing antibiotics (for 50 ml 45 ml D-MEM high glucose [4,5 g/ l D-MEM high glucose with L-glutamine] was supplemented with 25000 U/ ml penicillin and 25 mg/ ml streptomycin [PAA, Pasching, Austria], 5 ml heat-inactivated FCS, 1 M $MgCl_2$, and 125 µl NUTS [Nutrients]. NUTS contained 50 mg/ 10 ml ITS [insulin:transferrin:Na-selenite = 25:25:0.025; Roche Diagnostics, Mannheim, Germany] to which 100 nM progesterone and 100 µM putrescine were added [Sigma-Aldrich, Vienna, Austria]).

The solution was triturated with the aid of three Pasteur pipettes of decreasing opening diameters until a single cell suspension of hippocampal cells was achieved. Next the cell density was determined using a haemocytometer (cell counting chamber) and the required volume of cell suspension for a certain cell density was pipetted into a glass ring on PDL (Poly-D-Lysine; Sigma-Aldrich, Vienna, Austria)-coated 35 mm cell culture dishes. PDL was used to achieve better cell adhesion and the glass rings were necessary to warrant that the neurons are concentrated in the middle of the culture dishes. This is important to yield better access of the patch electrode and the application device in later electrophysiological experiments. The glass rings were removed after one to two hours, after adhesion was completed.
On the next day culture medium was replaced by antibiotic-free D-MEM medium to avoid possible side-effects of the antibiotic agents on neuronal functions. ARA-C (Cytosin-β-D-arabinofuranosid hydrochloride; Sigma-Aldrich, Vienna, Austria), an antimitotic drug necessary to limit the overgrowth of neurons by glial cells, was added to the cultures after 4 days. From then on the neurons were kept in the incubator at 37°C with 5 % $CO_2$ until use. Volume loss because of evaporation was compensated by adding 200 µl of autoclaved and sterile-filtered deionized water per week.

### 2.2 Solutions and drugs for electrophysiological recordings

The outer solution contained 140 mM NaCl, 3 mM KCl, 2 mM $CaCl_2$, and 2 mM $MgCl_2$, 10 mM HEPES (a buffer to control the pH), and 20 mM glucose (for balancing the osmolarity). NaOH was used to adjust the pH to 7,4.
The internal (pipette) solution contained 120 mM potassium gluconate, 1,5 mM sodium gluconate, 3,5 mM NaCl, 1,5 mM $CaCl_2$, 0,25 mM $MgCl_2$, 10 mM HEPES, 10 mM glucose, and 5 mM EGTA (which is a $Ca^{2+}$ chelator for quenching calcium ions). Finally, pH was adjusted to 7,3 using KOH.
The dihydropyridines Bay K 8644 (BayK; LTCC agonist) and isradipine (LTCC antagonist) were used at concentrations of 3 µm in my experiments to modulate the activity of L-type voltage-gated calcium channels. Both drugs were dissolved in dimethyl sulfoxide (DMSO) and this lipophilic solvent diluted in external solution itself served as control solution in my experiments. Furthermore, tetrodotoxin (TTX; Latoxan, Valence, France), a blocker of voltage-gated $Na^+$ channels, was used at concentration of 500 nM in current injection experiments. All ingredients for

preparation of external and internal solution, as well as BayK, isradipine, and DMSO were purchased from Sigma-Aldrich (Vienna, Austria).

### 2.3 Patch clamp setup and preparation for electrophysiological recordings

Patch pipettes (PP) were made from borosilicate capillaries (Science Products GB 150-8P, dimensions 0,86 x 1,50 x 80 mm) with a Sutter P-97 horizontal puller (Novate, CA, U.S.A.). Only patch electrodes with a resistance between 3 and 5 MΩ were used for my experiments. In order to avoid contamination of these micropipettes it was necessary that they were made and used immediately before starting an experiment and to store them in dust-free batches.

The tip of the pipette was then submerged into internal solution for about 5 seconds, leading to absorption of the solution due to capillary forces, and was backfilled with the same solution containing amphotericin B by using a thin quartz glass pipette. Air bubbles were removed from the micropipette by gently tipping against its glass wall. Thereafter it was mounted in a micropipette holder connected to a micromanipulator (Luigs and Neumann SMI/ Mini 25). Besides allowing movement of the pipette in three different axes, this device connects the pipette to a preamplifier (PA, Axon Instruments CV-7BO) via an Ag/ AgCl electrode. A reference (bathing) electrode (RE), which is needed to close the electrical circuit, also consisted of Ag/ AgCl and was placed within the culture dish. From the preamplifier the recorded signals were transmitted to a Multiclamp 700B amplifier (A, Axon Instruments), which was controlled with a personal computer (PC) via the Multiclamp 700B commander software (Axon Instruments). The analogous measurements were converted into digital form using a Digidata 1440A digitizer (DIGI, Axon Instruments) and recordings were made via Clampex 10.2 software (Axon Instruments).

For selection and visual observation of the neurons an inverse microscope (Nikon Eclipse TE3000) with 100 to 400fold magnification and phase-contrast was employed. A superfusion system (DAD-12, ALA, Scientific Instruments) containing 12 tubes converging into a single application tip was used for application of substances and drugs. The whole setup was mounted onto an anti-vibrating table (TMC, Micro-g 63-564) dampened with compressed air. A Faraday Cage (FC) was used for shielding the setup from electronic disturbances (Fig.7).

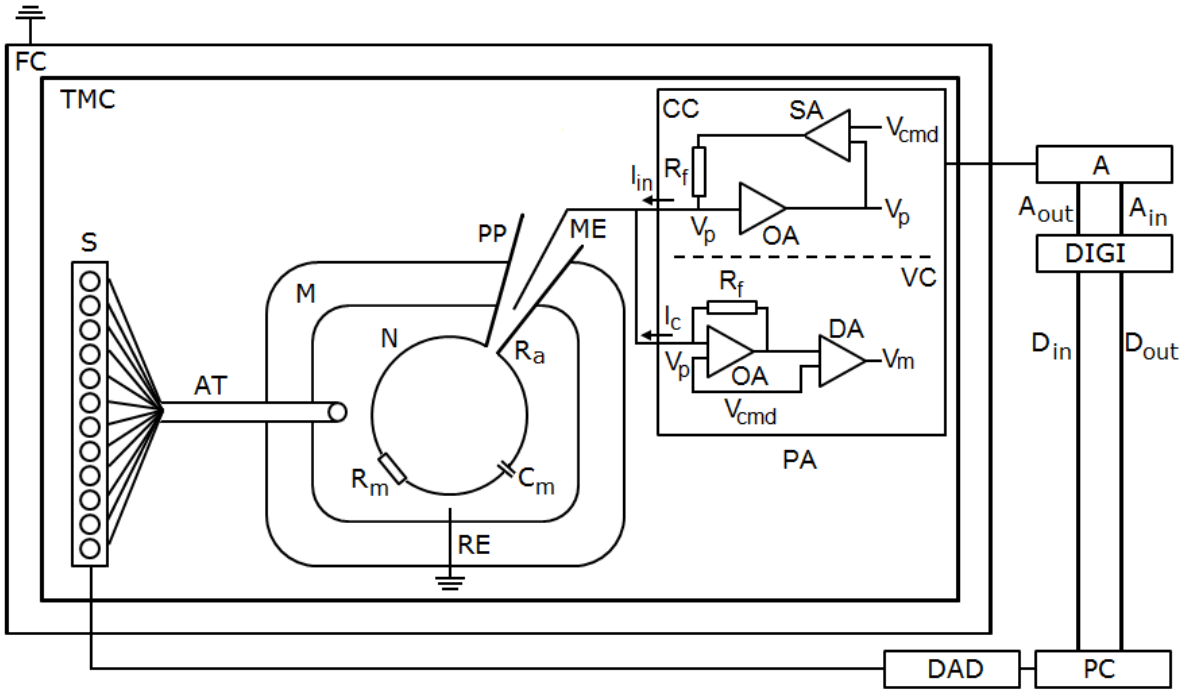


**Figure 7:** Experimental setup for electrophysiological recordings. A = amplifier , AT = application tip, CC = current clamp circuitry, $C_m$ = membrane capacitance, DA = differential amplifier, DAD = DAD superfusion system, DIGI = digitizer, FC = Faraday cage, $I_c$ = compensatory current, $I_{in}$ = injected current, M = microscope table, ME = microelectrode, N = neuron, OA = operational amplifier, PA = preamplifier, PC = personal computer, PP = patch pipette, $R_a$ = access resistance, RE = reference electrode, $R_f$ = feedback resistor, $R_m$ = membrane resistance, S = superfusion device, SA = summing amplifier, TMC = compressed air dampened table, VC = voltage clamp circuitry, $V_{cmd}$ = command potential, Vm = membrane voltage, $V_p$ = pipette voltage (modified according to Numberger and Draguhn, 1996; Molleman, 2003; Sherman-Gold, 2006; Okada, 2012).

The application tip was positioned in such a way that it could just be seen in the periphery of the visual field of the microscope at largest magnification and neurons were continuously superfused with external solution at a pressure of 200 Pa (Fig.8).

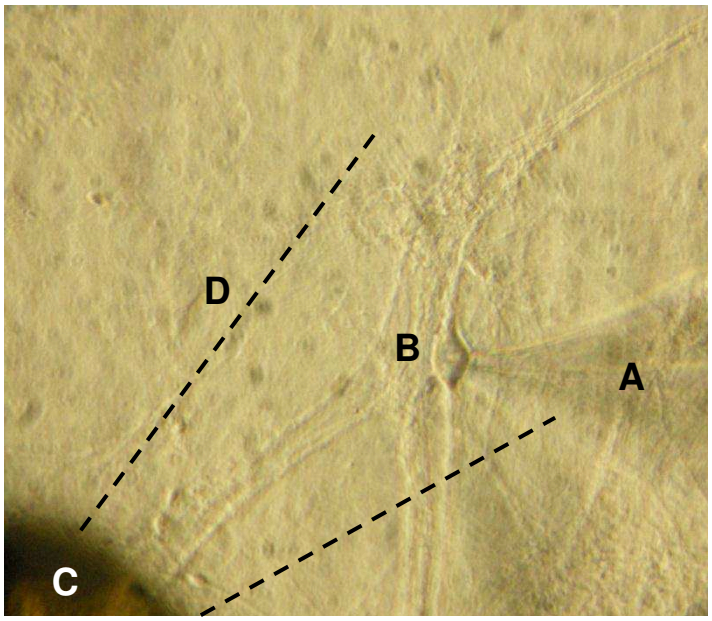


**Figure 8:** Neuron in an experimental situation. Lowering of the microelectrode (A) onto the membrane of a target neuron (B) leads to a connection between them, which is further strengthened via application of suction. Since the pipette is filled with internal solution and amphotericin B, pores are generated in the membrane, which allows electrical access to the cell's interior. The neuron is positioned in front of an application tip (C) to warrant superfusion (D) of the cell with different solutions and drugs.

Immediately before starting an experiment, culture dishes were taken out of the incubator, washed once with external buffer solution, and filled with 2,25 ml of the same buffer. Amphotericin B stock solution (50 mg/ ml) was diluted 1:100 into the inner solution. All experiments were performed at room temperature (~ 25°C).

### 2.4 Patch clamp recording modes

The patch clamp technique offers two possible recording modes. In the voltage clamp (VC) the membrane voltage is set by the experimenter ($V_{cmd}$, command potential) and this allows direct recording of the membrane current at this voltage (Hille, 2001; Molleman, 2003; Sherman-Gold, 2006). The command potential is then compared with the measured potential ($V_p$). Deviations between both voltages are corrected via an electronic feedback system by injection of a compensatory current ($I_c$) that mirrors the ionic current over the membrane (Molleman, 2003).
In contrast, in current clamp (CC) mode the experimenter can directly measure the membrane potential ($V_p$), and, thus, the electrical activity of a neuron. It is also possible to inject a constant amount of current ($I_{in}$) to alter the membrane potential experimentally (Molleman, 2003; Sherman-Gold, 2006) (see circuitries in Fig.7).

#### 2.4.1 Perforated-patch recording

After achieving a stable connection between the micropipette and the cell membrane (a so called “seal”), the perforated-patch mode was employed to gain access to the cell’s cytosol. This method allows good electrical access to the neuron’s interior, which is left largely unaffected, and therefore is much less invasive compared to the whole-cell mode (Horn and Marty, 1988; Hille, 2001; Molleman, 2003; Sherman-Gold, 2006). The perforated-patch mode can be achieved by the use of ionophores, which are able to form electrically conductive aqueous pores in cholesterol- or ergosterol-containing membranes. Nystatin (derived from *Streptomyces nousei*) and amphotericin B (derived from *Streptomyces nodosus*), structurally similar polyene antibiotics, are two examples of such perforating agents. Both contain an amphipathic polyhydrophilic lactone ring that interacts with sterols in the membrane to form a barrel-like pore (~ 0,4 – 0,5 nm). Monovalent cations are small enough to permeate through these channels, whereas multivalent ions such as $Ca^{2+}$ or $Mg^{2+}$ are

excluded. $Cl^-$ ions can also pass through pores formed by nystatin or amphotericin B, however, nine times less effective than monovalent cations. In contrast gramicidin, a linear polypeptide antibiotic derived from *Bacillus brevis*, creates pores of ≤ 0,35 nm, which are only permeable to univalent cations and thus can be used to maintain the intracellular anion concentration. Molecules larger than glucose (~ 0,8 nm) or sucrose (~ 1 nm) will not permeate through these pores and therefore the experimenter can prevent washout of important second messengers (e.g. cAMP, ATP, intracellular $Ca^{2+}$) as well as proteins important for cell signalling or regulation of channels (Hille, 2001; Molleman, 2003; Sherman-Gold, 2006; Zhao et al., 2009; Okada, 2012).

Amphotericin B, which was used in our experiments, has limited water solubility and was therefore solubilised in DMSO. Furthermore, it is light sensitive and thus was kept under light protection. Before every measurement the amphotericin B stock (50 mg/ ml) was freshly diluted into internal solution (1:100) and was solubilised by vortexing and sonication.

For successful sealing it is important that the perforating agent should not be applied before a seal is formed. To cancel out this possibility the pipette was first submerged into internal solution for about 5 seconds, leading to absorption of the solution due to capillary forces, before it was backfilled with the same solution containing amphotericin B. This allows for a gradually timed introduction of the perforating drug onto the pipette patch.

## 2.5 Measuring of a target neuron

### 2.5.1 Approaching the neuronal membrane and pipette offset correction

After changing the media of a culture dish and putting it into its appropriate position under the microscope, a target neuron was chosen. Then a microelectrode filled with internal solution and internal solution containing amphotericin B was fixed in the electrode holder. Before lowering the pipette into the bathing solution it is necessary to keep the tip free from contaminations in the bathing solution (e.g. cell debris). This can be achieved by the use of a tubing system, which is connected to the microelectrode holder via an auxiliary channel and which can be controlled via a mouthpiece. Since this U-shaped tube is filled with water, the experimenter can put a

slight positive pressure on the pipette to avoid stuffing of the pipette tip by possible contaminations (Fig.9A).

In order to approach the microelectrode to the cell membrane, the pipette was lowered into the bathing solution in VC mode using App_Ch1.pro [command potential ($U_0$) = 0 mV]. As a response to a 100 ms long voltage step (ΔU) of 5 mV with a frequency of 5 Hz, a rectangular current (I) could be observed in Clampex 10.2, which marks the pipette resistance ($R_p$) (Fig.9A). $R_p$ then was automatically calculated by the software according to Ohm's law: U = R • I.

Since the holding potential is 0 mV ($U_0$ = 0 mV), there should be no current present between the bathing electrode and the measuring pipette at this time point. However, due to offset potentials of various origins there are always fluctuations. These can be redox reactions (electron transfer) between the metals of both electrodes and the ions in the solution (solid-liquid junction potentials). Furthermore, accumulation of ions near the electrodes (polarization) or differences in the mobility and concentration between different solutions (liquid junction potentials) may contribute to these offset potentials. Hence, the use of a bathing and a measuring electrode which are identical according to their type of material and maintenance of the AgCl layer on the outside of the pipette, can help to reduce these fluctuations (Molleman, 2003). With the Multiclamp 700B commander one can conveniently compensate this pipette offset potentials via the pipette offset knob. This ensures that the command potential will correctly be applied to the membrane.

### 2.5.2 Compensation of capacitive artefacts and seal formation

The pipette was then lowered towards the membrane of the target neuron under visual examination and shortly before touching it a "sweep" (screenshot of the recent current transient) was stored. This is important to detect a drop of the current response, which signifies an increase in pipette resistance due to occlusion of the pipette tip by the cell membrane. Further decrease of the current, marking stronger connection between the microelectrode and the membrane, was achieved through application of delicate suction on the microelectrode. This is done until the electrical resistance between the inside and outside of the electrode, called leak resistance, yield values near 1 GigaOhm ("gigaseal") (Okada, 2012). Holding currents then amount to ≤ 100 pA (Fig.9A).

### 2.5.3 Getting electrical access to the cell's interior

The program then was switched to Break_Ch1.pro, where the neuron is held at a holding potential of -70 mV and a voltage step of 10 mV is applied.

In electrical terms a capacitor is described as an insulator between two conducting layers. Thus, the glass wall of the pipette, which builds an insulator between pipette and bathing solution (two conductors), can be considered a capacitor. It gets charged with every change in holding potential and this can be detected as so called "capacitive transients" in the current traces (Molleman, 2003). By using Multiclamp 700B these artefacts can be cancelled out using compensation knobs ($C_p$ slow, $C_p$ fast).

Because of the light sensitivity of amphotericin B, the light source of the microscope was then turned off and a sweep was stored in Clampex 10.2 to follow the re-manifestation of capacitive transients, which represents pore formation. Reoccurrence of transients, and therefore access to the cell's interior, was achieved after about 10 to 15 minutes [Fig.9B]. In order to record electrical activity the program was switched to current clamp continuous.pro. To warrant that viable neurons were included into this study, only cells with a membrane potential more negative than -50 mV, which generated over-shooting action potentials (shooting beyond 0 mV), were used for the experiments.

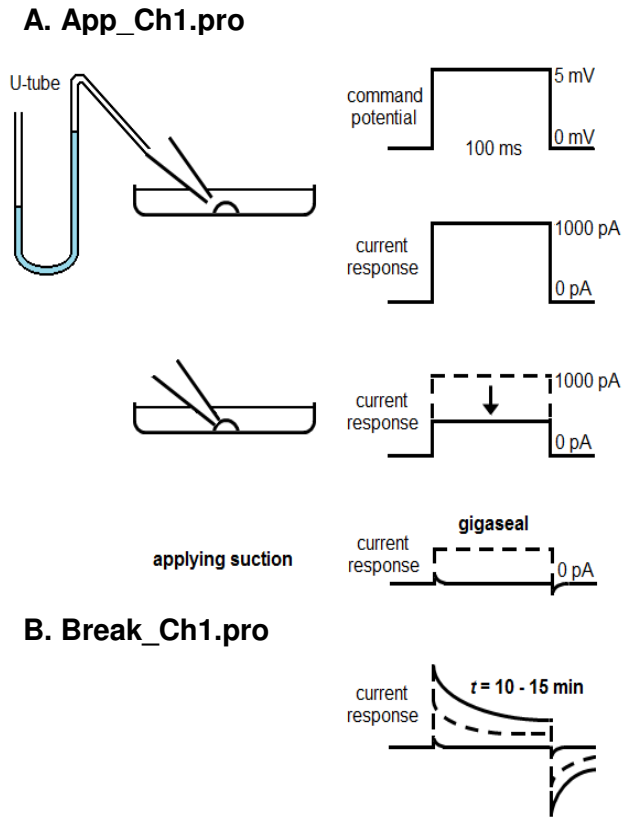


**Figure 9:** Overview of the principal steps to monitor stable seal formation and electrical access to the cell's interior. In the approach program (App_Ch1.pro) the pipette is lowered onto the membrane of a target neuron. Positive pressure is put onto the microelectrode via an U-shaped tubing system to avoid stuffing of the microelectrode tip by possible contaminations in the bathing solution. Contact between the membrane and the pipette tip becomes visible by a drop of the current response to a voltage step of 5 mV for 100 ms. Through suction a gigaseal is established. B. After making a voltage step of 10 mV and stepping back to a command potential of -70 mV (Break_Ch1.pro) capacitive transients occur, which are cancelled out automatically in Multiclamp 700B. Growing accessibility to the cell's interior can be followed by a re-manifestation of capacitive transients, which is achieved after 10 to 15 minutes (modified according to Molleman, 2003).

## 2.6 Experimental design to study the role of excitatory or inhibitory coupling in neuronal excitability

Three different firing modalities of a neuron can be observed in current clamp mode. Cells can be grouped into: (I) silent cells, (II) tonic firing cells, or (III) bursting (phasic firing) cells. Traces recorded from neurons of group I solely display excitatory (EPSPs) or inhibitory postsynaptic potentials (IPSPs). However, sometimes single action potentials are visible when these EPSPs are large enough to reach the action potential threshold. In contrast, tonic firing (II) denotes a situation, in which neurons show a regular or irregular sequence of action potentials. These cells additionally can display EPSPs or IPSPs. Neurons of group III show phasic discharge patterns as described in subchapter 1.3.3 and Fig.5.

In this study, I wanted to investigate the influence of currents underlying after-depolarizations or after-hyperpolarizations on neuronal electrical activity, i.e. if these currents are involved in the modulation of action potentials, EPSPs, IPSPs, or burst events. Hence, only recordings from neurons, which display tonic or burst firing were used in my experiments and electrical activity of each neuron was measured for 3 minutes in the presence of the LTCC agonist BayK (Fig.10A).

In a following step current pulses of variable strength, depending on the membrane resistance of the respective cell, were injected to depolarize the cells to the activation threshold of LTCCs. In this way it was possible to determine if an ADP- or AHP-generating neuron was recorded from. In a previous study of our group it was described that after-depolarizations were elicited with shorter pulses, whereas after-hyperpolarizations could be induced by longer current injections (Geier at al., 2011). Hence, to warrant that both after-potentials could be induced properly, two different protocols of variable pulse durations were employed. In the first program (MR deltadur short.pro) four brief stimuli, of which each was prolonged by 250 ms compared to the previous one (starting from 50 ms and finally reaching 800 ms), were injected (Fig.10B1+C1). The second protocol (MR deltadur long.pro) contained 3 longer-lasting pulses, which increased 1 s in duration with every injection (starting from 1 s and finally reaching 3 s) [Fig.10B2+C2]. The influence of LTCCs on after-potentials was determined using the LTCC agonist BayK and the LTCC antagonist isradipine. Additionally, tetrodotoxin (TTX) was applied to the neurons to avoid

activation of voltage-gated sodium channels. In all of these current injection experiments the lipophilic solvent DMSO was used as a control.

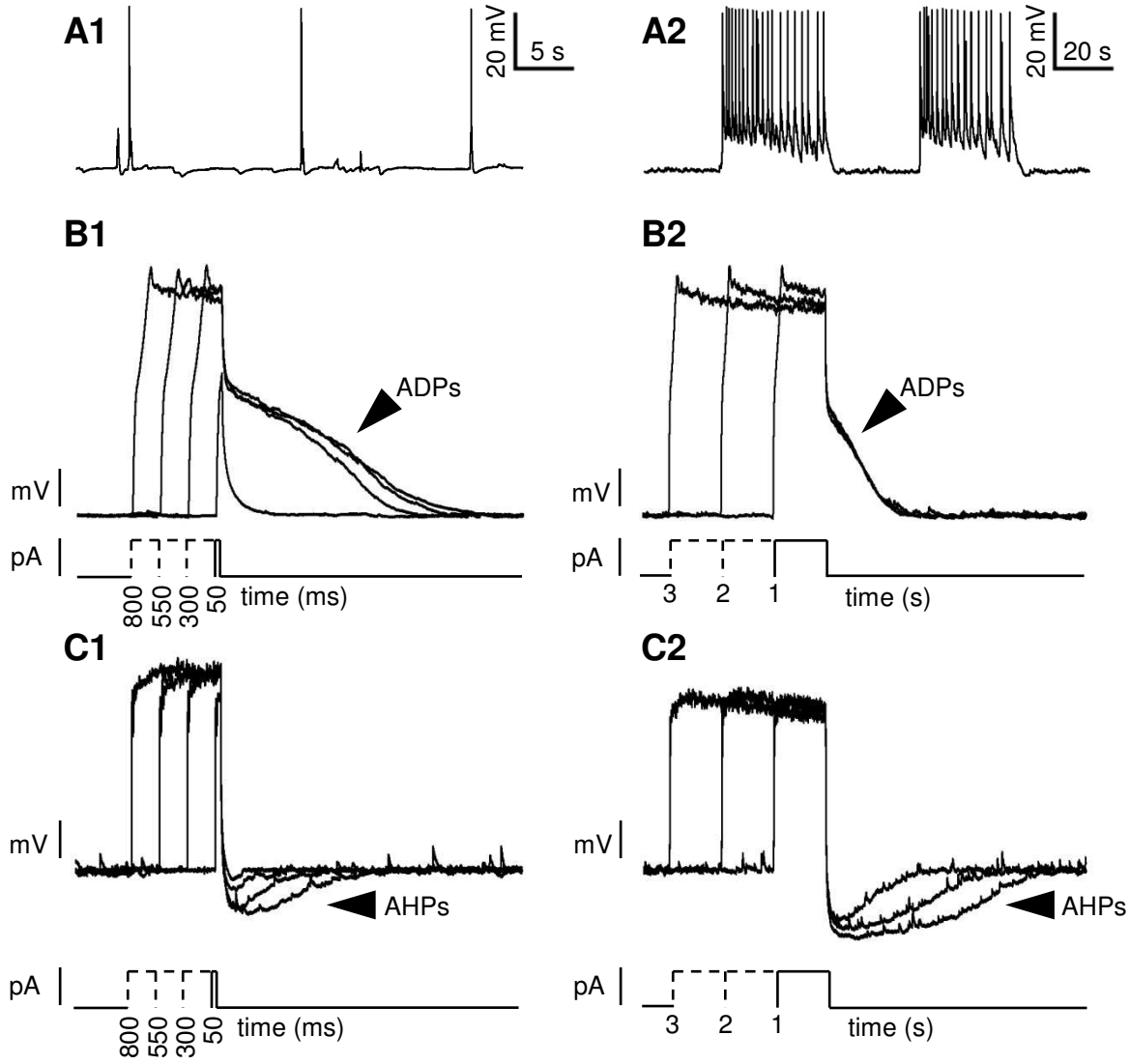


**Figure 10:** Protocols to study the influence of after-potentials on neuronal electrical activity. A. Current clamp recordings of tonic (A1; spike events, EPSPs, and IPSPs are visible in this example trace) or bursting (A2) neuronal activities were made in the presence of the LTCC agonist BayK. B. + C. Test for after-potentials in the respective neurons using current injections when the action potential blocker tetrodotoxin and BayK or isradipine (LTCC antagonist; not shown) were applied. Brief (B1, C1) and long current pulses (B2, C2) were employed to warrant optimal induction of ADPs (B1, B2) or AHPs (C1, C2).

### 2.6.1 Dependence of after-potentials and firing modes on resting membrane potential

In my recordings 21 neurons showing no distinct after-potential (I), 26 ADP-generating neurons (II), and 24 neurons with an AHP (III) were observed. The

median membrane voltage of cells lacking after-potentials amounted to -65 mV± 8,6 mV. In ADP-generating neurons (-70 mV ± 9,8 mV) and AHP-generating neurons (-70 mV ± 8,8 mV) similar findings were observed (Fig.11A). Hence, whether neurons lack a distinct after-potential or generate an ADP or AHP does not depend on their membrane voltage.

In contrast, comparison of resting membrane potentials of all tonic (n = 32) and all bursting neurons (n = 39) in the three experimental groups (I – III) revealed that membrane voltage has an impact on the neuronal firing pattern. On average tonic firing neurons (-60 mV ± 6,3 mV) were 12,5 mV more depolarized than bursting cells (-72,5 mV ± 6,4 mV) [Fig.11B]. See Fig.16 for examples.

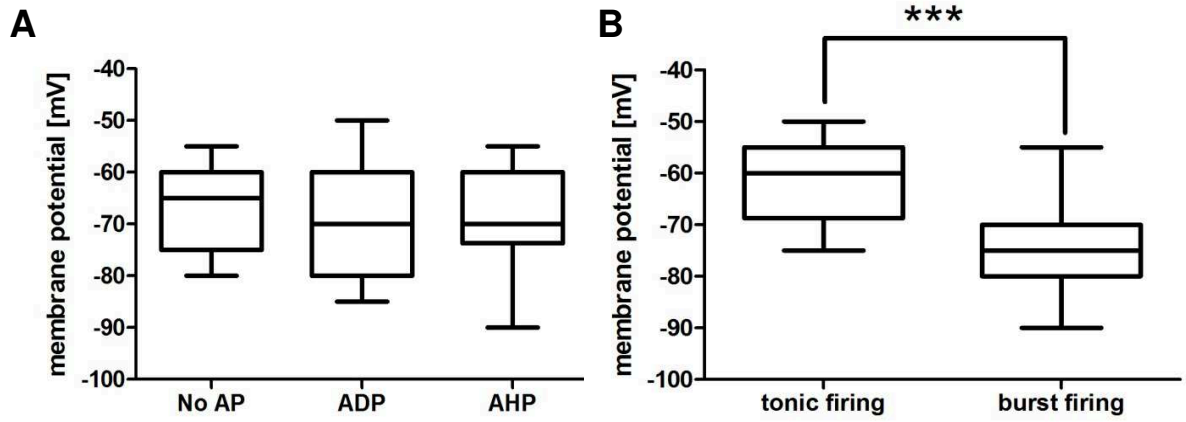


**Figure 11:** Comparison of resting membrane potentials between neurons with different after-potentials and firing modalities. A. No significant differences in the median membrane voltages between cells lacking an after-potential (n = 21), ADP-generating cells (n = 26), and AHP-generating neurons (n = 24) was detected. Statistical analysis was performed using One-way analysis of variance and comparison between the groups was carried out with Tukey's Multiple Comparison Test (p = 0,4637). B. A difference in the median membrane potentials of neurons which are either tonic firing (n = 32) or bursting (n = 39) was observed. Comparison between both groups was done using unpaired t-test. *** p < 0,001.

### 2.6.2 Dependence of the after-potential magnitude on stimulus duration

In order to investigate if the size of after-potentials depends on pulse duration, length of current injections was varied from brief (50 ms) to long (3 s) durations, as described in subchapter 2.6 and Fig.10. The size of the area-below-the trace (ABT) of ADPs and the area-over-trace (AOT) of AHPs was determined via comparison of traces recorded in the presence of BayK with those recorded under application of isradipine (Fig.12A+B). Not all of the 26 ADP-generating and 24 AHP-generating neurons remained viable during the current injection experiments when the LTCC

antagonist was applied. Only cells in which both pulse protocols could be carried out in the presence of BayK as well as isradipine were included into the analysis of the after-potential size. Thus, 19 BayK-induced ADPs and 20 BayK-induced AHPs at brief pulse durations (50 ms to 800 ms) and one more for both groups at longer pulse durations (n = 20 and n = 21, respectively) were used for this evaluation. In the presence of BayK the magnitude of ADPs reached its maximum with shortest pulses and declined with prolongation of the stimulus length. Contrary, after-hyperpolarizations became larger with increased pulse durations (Fig. 12C).

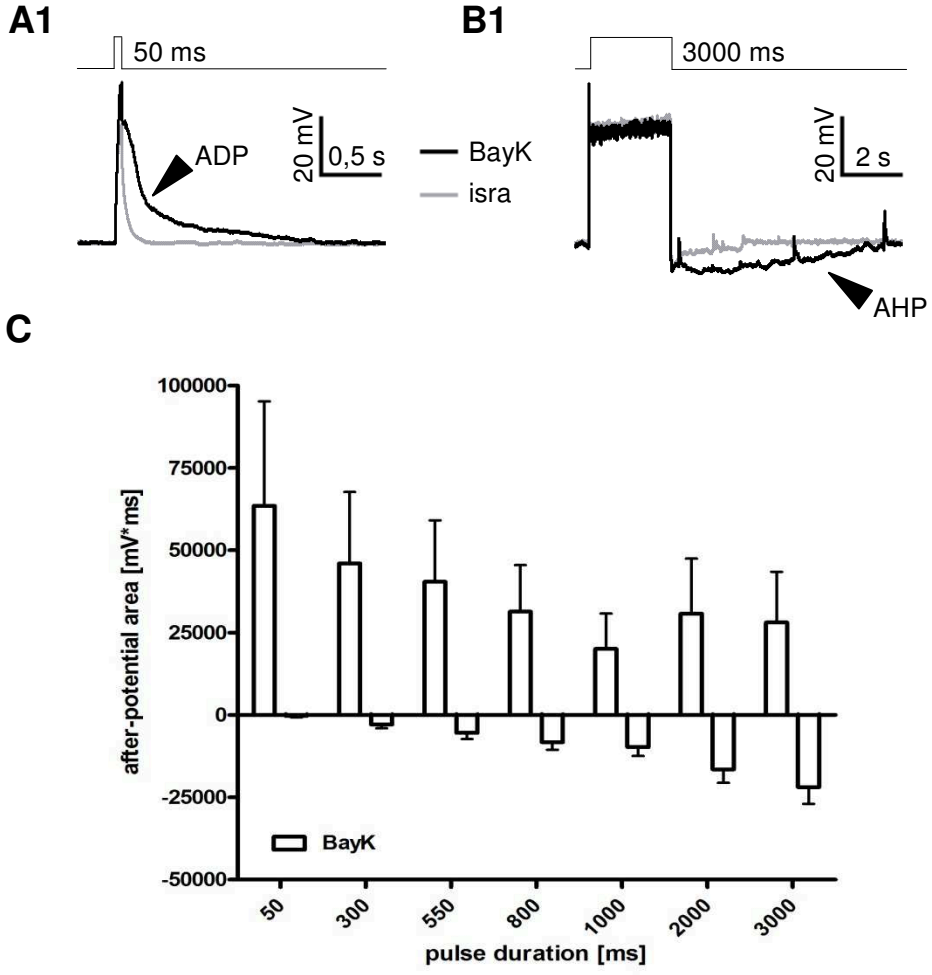


**Figure 12:** Dependence of after-potential size on stimulus length. After-potentials were elicited upon depolarization via brief (from 50 ms to 800 ms in 250 ms-steps) and long current injections (from 1 s to 3 s in 1 s-steps). A1. + B1. Sample overlays of recordings made in the presence of the LTCC agonist BayK (black traces) and the LTCC antagonist isradipine (grey traces) at shortest pulse durations (50 ms; A1) and longest pulse durations (3 s; B1). Arrowheads depict an after-depolarization (ADP; A1), which was evoked by brief current injections (50 ms), and an after-hyperpolarization (AHP; B1), which can be induced by longer lasting stimulation (3 s). C. Area of after-potentials (given as mV*ms) plotted against the pulse duration in the presence of the LTCC agonist (n = 19 and n = 20 at brief stimulus durations and n = 20 and n = 21 at longer lasting current injections for ADPs and AHPs, respectively). Bars are representations of means ± SEM of after-potential areas.

### 2.6.3 Dependence of after-potential size on age of cell culture

The next experiment was carried out to ensure that the occurrence and size of depolarizing and/ or hyperpolarizing after-potentials is independent from the age of the cell culture. Since my earliest recordings were done using 11 day (d) old cells and experiments, in some cases, could be carried out until day 34 after preparation, it was possible to analyse if age of primary neurons *in vitro* had an impact on the generation of after-potentials.

Comparison of the three experimental groups revealed that absence of after-potentials (n = 21; 18 d ± 2 d) or occurrence of ADPs (n = 26; 19,5 d ± 5 d) or AHPs (n = 24; 18 d ± 5 d) is not dependent on the age of cells in culture (Fig.13).

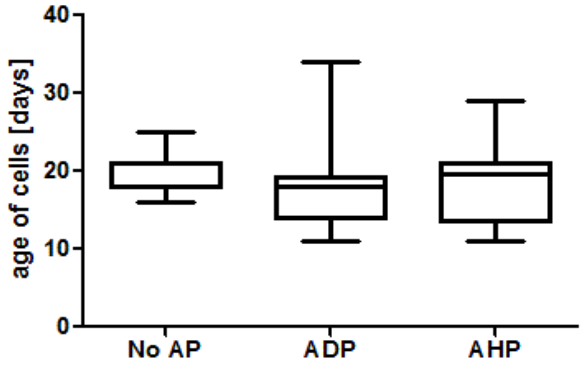


**Figure 13:** Independence of cells with different after-potentials on age of cells in culture (given as days after preparation). No significant difference in the median age between cells without an after-potential (No AP; n = 21), ADP-generating neurons (n = 26), and AHP-generating neurons (n = 24) could be detected. Statistical analysis was performed using Kruskal-Wallis test and comparison between the groups was done with Dunn's Multiple Comparison Test (p = 0,1734).

In a next step I investigated if the size of after-depolarizations and after-hyperpolarization depends on the age of the cultures. Hence, ABT of ADPs, which were most prominent at 50 ms current injections, and AOT of AHPs, which were greatest in size with 3 s stimuli, was plotted against the age of cells in vitro (again given as days after preparation). Size of after-depolarizations and after-hyperpolarizations was measured as described in subchapter 2.6.2. Again, only neurons in which it was possible to do current injection experiments in the presence of BayK and isradipine, were included into this study. Correlation analysis showed that size of after-depolarizations (n = 19) or after-hyperpolarizations (n = 21) is not dependent on the age of neurons *in vitro* (Fig.14).

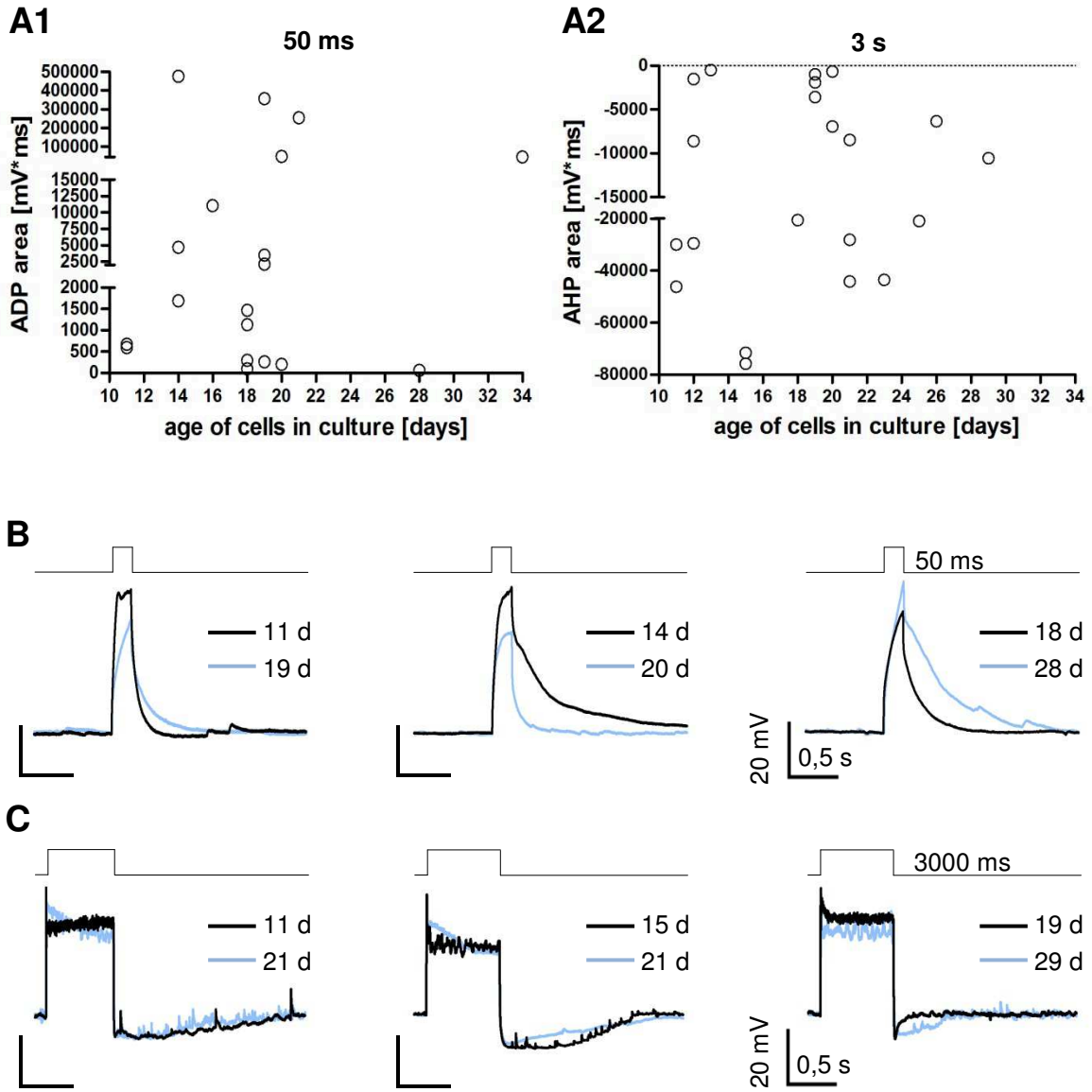


**Figure 14:** Age-independence of after-potential size. ABT of after-depolarizations at brief pulse durations (50 ms) and AOT of after-hyperpolarizations at longest current injections (3 s) [both given as mV*ms] were plotted against age of cells in culture (given as days after preparation). A. Spearman correlation analysis revealed that size of ADPs (n = 19; A1) in the presence of BayK is not age-dependent ($r_s$ = 0,04), and the same was observed with Pearson correlation analysis for AHPs (n = 21, $r$ = 0,2; A2). For better visualization of all data points gaps were inserted into the y-axis of A1 and A2. B+C. Sample overlays of after-depolarizations (B) and after-hyperpolarizations (C) from older (light blue) and younger (black) neurons in the presence of BayK. These examples show that young and aged neurons may be similar in size (left traces in B and C), that young neurons may achieve larger after-potentials (middle traces in B and C) or that older cells give rise to larger after-potentials (right traces in B and C).

## 2.7 Data analysis and statistics

### 2.7.1 Event detection analysis

Evaluation of area-below-trace (ABT) of burst events, action potentials (also referred to as “spike events” in this study), and excitatory postsynaptic potentials (EPSPs), as well as area-over-trace (AOT) of inhibitory postsynaptic potentials (IPSPs) was done using event detection operation in Clampex 10.2. To warrant that this analysis is done under the same conditions for all the neurons included into this study, the baseline membrane potential of the recorded neuronal activities was set to 0 mV via baseline adjustment and a baseline marker (0 mV) was set onto it. Furthermore, a trigger marker was set to 5 mV for tonic firing cells and to 15 mV for bursting cells and a re-arm marker to 0,5 mV for both firing patterns. An event is considered to start when the membrane potential from below the re-arm value exceeds the trigger marker and its end is determined when it falls below the latter marker again. The ABT (given as mV*ms) of such an event is then calculated by Clampex 10.2. For analysis of AOT (given as mV*ms) of IPSPs the trigger marker was set to -5 mV and the re-arm marker to -0,5 mV (Fig.15). In order to avoid confusion of “spike events” with EPSPs, only excitatory postsynaptic potentials, which did not exceed the threshold for action potential firing (thus, remained below -50 mV), were included into this study.

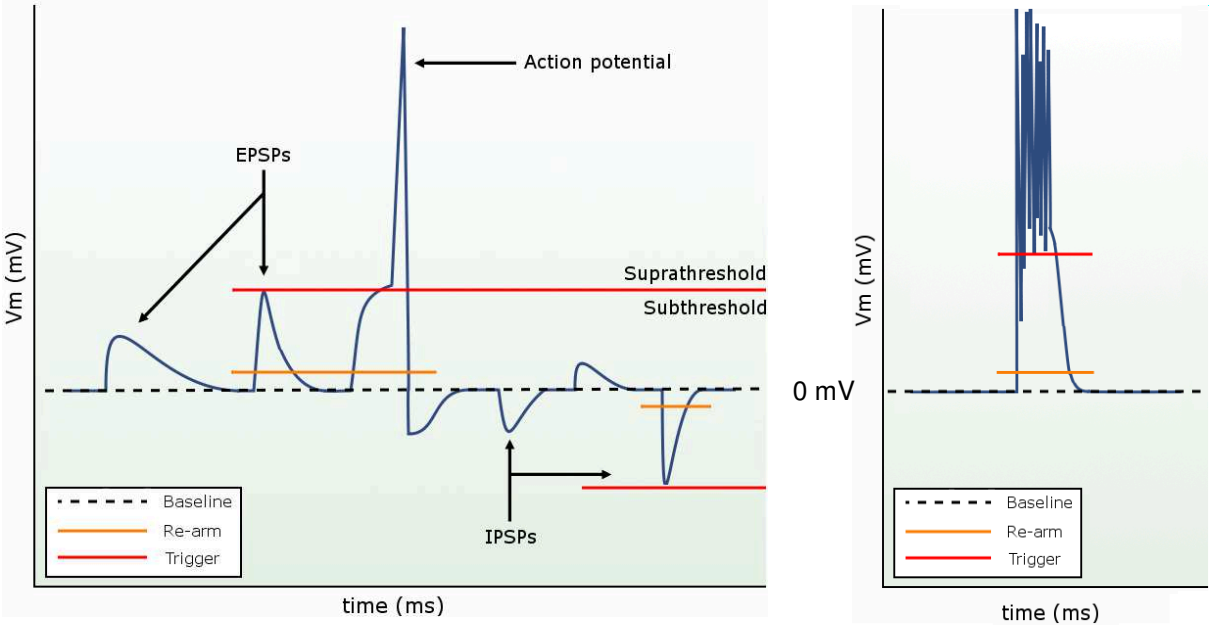


**Figure 15:** Experimental design to determine area-below-trace of burst events, action potentials, and EPSPs, as well as area-over-trace of IPSPs. In a first step the baseline of all traces was set to 0 mV. An event is identified when the membrane voltage exceeds both, the re-arm and the trigger marker, and then undershoots the trigger marker again.

### 2.7.2 Statistical comparison between groups and graphical illustrations

All statistical tests were performed with GraphPad Prism 5. Additionally, all diagrams were created using this software. Before statistical analysis was carried out, D'Agostino-Pearson omnibus test was employed to test for normal distribution of the data. The f-test was employed to test for homogeneity of variances in two groups containing normally distributed values. When homogeneities of variances between these groups did not differ significantly, they were compared using unpaired t-test. One-way analysis of variance (ANOVA) with a subsequent Tukey's Multiple Comparison Test was carried out to determine differences between three groups. Two groups containing data, which were not normally distributed, were compared using Mann Whitney Test. For statistical analysis of three groups Kruskal-Wallis test followed by Dunn's Multiple Comparison Test was performed. Correlation analysis was carried out in the case of normally distributed data using Pearson correlation analysis (results are given as Pearson rank correlation coefficient $r$), and in the case of not normally distributed data using Spearman correlation analysis (results are given as Spearman correlation coefficient $r_s$).

# 3. RESULTS

## 3.1 Distribution of tonic and burst firing in neurons with different after-potentials

Current injections of different strengths were used to depolarize the neurons to the activation threshold of LTCCs. The cells were continuously superfused with 0,5 µM TTX to avoid activation of voltage-gated $Na^+$ channels. The influence of LTCCs on pulse injection-induced after-potentials was confirmed by comparison of recordings made in the presence of 3 µM BayK with recordings, made in the presence of the LTCC antagonist isradipine (also at 3 µM). Furthermore, DMSO was used as a control in these experiments. In some neurons current injections could only be done in the presence of the LTCC agonist because, when superfused with isradipine, these cells were not viable anymore. Nevertheless, these measurements were included into this study if a prominent ADP or AHP was elicited upon BayK application.

In this way I identified 21 cells which did not give rise to a distinct after-potential (I; No AP) when superfused with the LTCC agonist. Contrary, 26 neurons showed an after-depolarization (II) and 24 neurons generated an after-hyperpolarization (III) upon pulse injections when BayK was applied.

Electrical activity of the neurons in these three experimental groups (I – III) was determined in the presence of the LTCC agonist. The distribution of tonic and burst firing was quite similar between after-potential lacking cells and cells showing an AHP (52% tonic firing vs. 48% bursting cells and 50% tonic firing vs. 50% bursting cells, respectively). However, burst firing predominated in neurons which generated an ADP upon application of BayK (35% tonic firing vs. 65% bursting neurons) [Table 2, Fig.16].

| | No AP | ADP-generating neurons | AHP-generating neurons |
|---|---|---|---|
| Number of cells; n | 21 | 26 | 24 |
| Tonic firing; n (%) | 11 (52) | 9 (35) | 12 (50) |
| Burst firing; n (%) | 10 (48) | 17 (65) | 12 (50) |

**Table 2:** Total numbers of neurons in the three experimental groups and distribution of tonic firing and bursting in the respective cells. Numbers in parentheses depict overall percentage of discharge patterns in the respective groups. No AP = no after-potential.

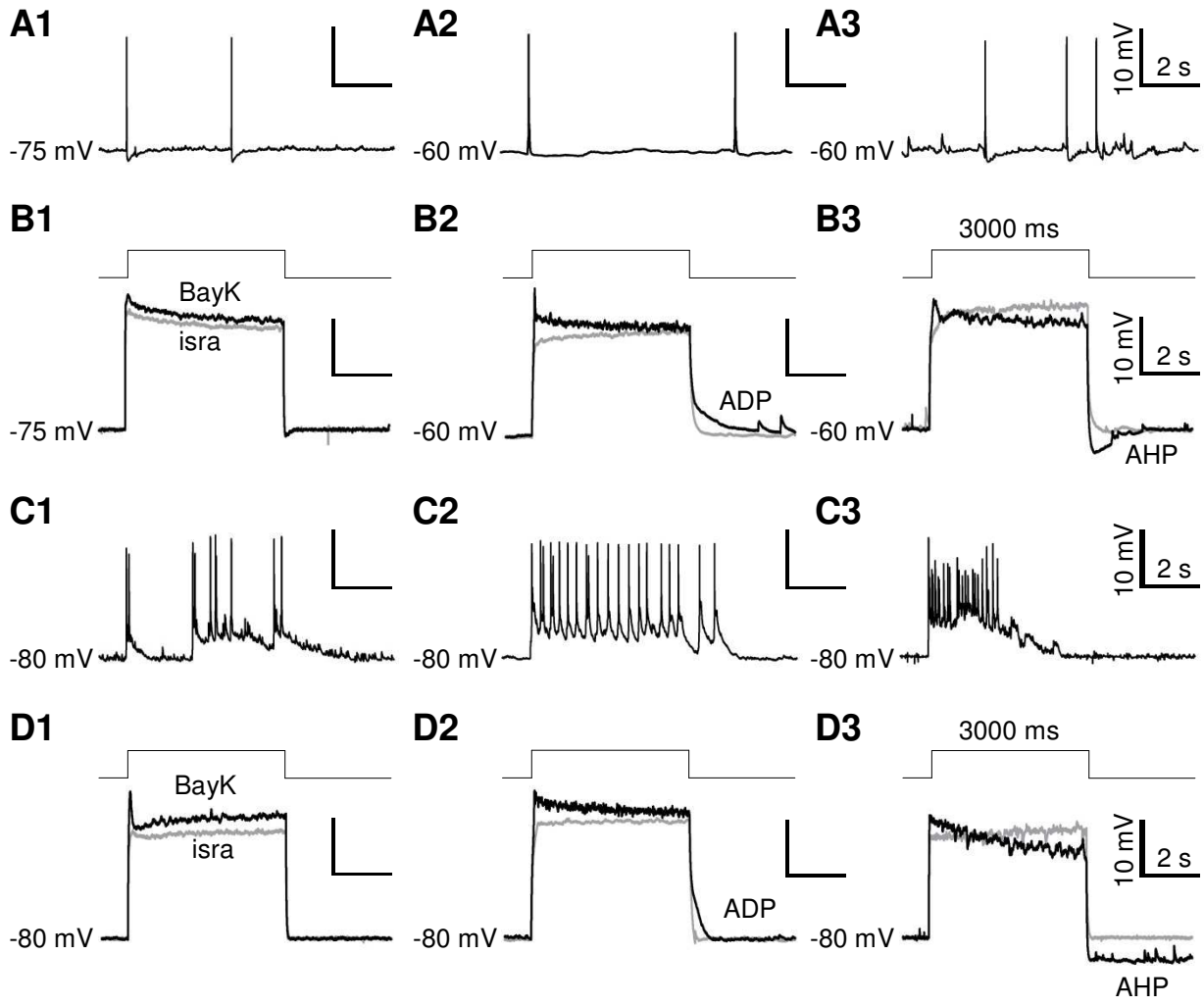


**Figure 16:** Electrical activity in neurons with different after-potential patterns. Sample recordings of tonic (A) and burst firing (C) traces in the presence of BayK from neurons lacking an after-potential (A1 - D1), in ADP-generating neurons (A2 - D2), and in AHP-generating neurons (A3 - D3). After-potentials were identified via current injections in the presence of tetrodotoxin (TTX), the LTCC agonist (black traces in B and D), and the LTCC antagonist isradipine (grey traces in B and D).

## 3.2 Distribution of active LTCC-mediated voltage responses in neurons with different after-potentials

All of the active LTCC-mediated voltage responses, which were described in a previous publication of our group (Geier et al., 2011), were similar to those observed in my recordings (Fig.17).

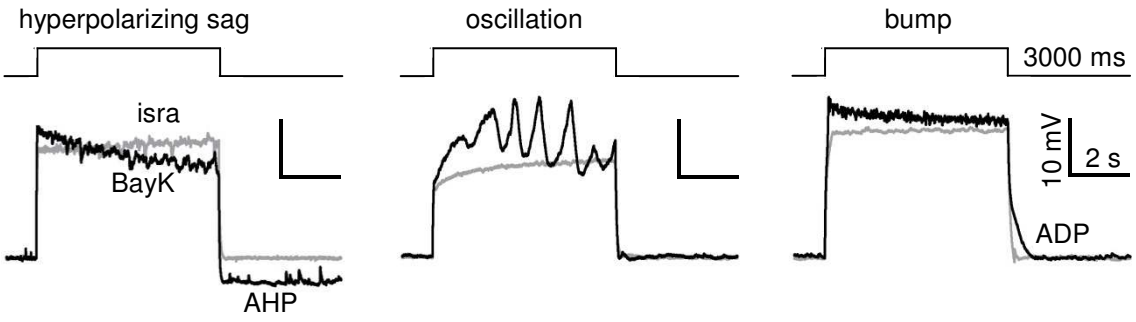


**Figure 17:** Samples of LTCC-mediated active voltage responses, which were elicited via current injections. Tetrodotoxin was used in these experiments to avoid activation of voltage-gated sodium channels. In presence of the LTCC agonist BayK all of the 3 active voltage responses, namely hyperpolarizing sags, oscillations, and bumps could be identified in the recordings, which disappeared in traces in which the LTCC antagonist isradipine was applied.

Bumps predominated in ADP-generating neurons (65,5 %), whereas hyperpolarizing sags yielded highest frequency distribution in those neurons showing a LTCC-mediated after-hyperpolarization (50 %). A considerable percentage of cells that lack an after-potential also showed no evident voltage response (33 %). When a voltage response was discernible it was in the form of oscillatory activity (28.5 %) or bumps (24 %). Interestingly, oscillations could also be detected in neurons generating an AHP (25 %), but were completely missing in cells with a LTCC-mediated after-depolarization (Table 3).

| LTCC-mediated voltage response | No AP n (%) | ADP-generating neurons n (%) | AHP-generating neurons n (%) |
|---|---|---|---|
| Hyperpolarizing sag | 2 (9.5) | 3 (11.5) | 12 (50) |
| Oscillation | 6 (28.5) | 0 | 6 (25) |
| Bump | 5 (24) | 17 (65.5) | 2 (8.3) |
| No response | 7 (33) | 0 | 2 (8.3) |
| n.A. | 1 (5) | 6 (23) | 2 (8.3) |

**Table 3:** Distribution of LTCC-mediated voltage responses in neurons lacking an after-potential (No AP) and in neurons with after-depolarizations or after-hyperpolarizations**.** n.A. (not available) represents cells in which current injection experiments could only be done with the LTCC agonist but not in the presence of isradipine. Numbers in parenthesis represent percentages of active voltage responses in the three experimental groups.

### 3.3 Effect of currents underlying depolarizing or hyperpolarizing after-potentials on burst firing

The ABT of burst events was determined via event detection analysis in the presence of the LTCC agonist BayK and was compared between neurons which did not elicit a distinct after-potential and ADP- and AHP-generating neurons. This was done to test for differences in burst size among cells with depolarizing or hyperpolarizing after-potentials.

The depolarization wave underlying burst firing was significantly increased in ADP-generating neurons compared to those showing an AHP in the presence of BayK. No differences could be observed in ABT of bursts when cells lacking an after-potential where compared with the other two experimental groups. However, a tendency towards augmented burst firing in ADP-generating neurons compared to neurons without any distinct after-potential could be detected, whereas a trend towards a reduction of burst events was identified in AHP-generating neurons as compared to neurons showing no distinct after-potential (Fig.18).

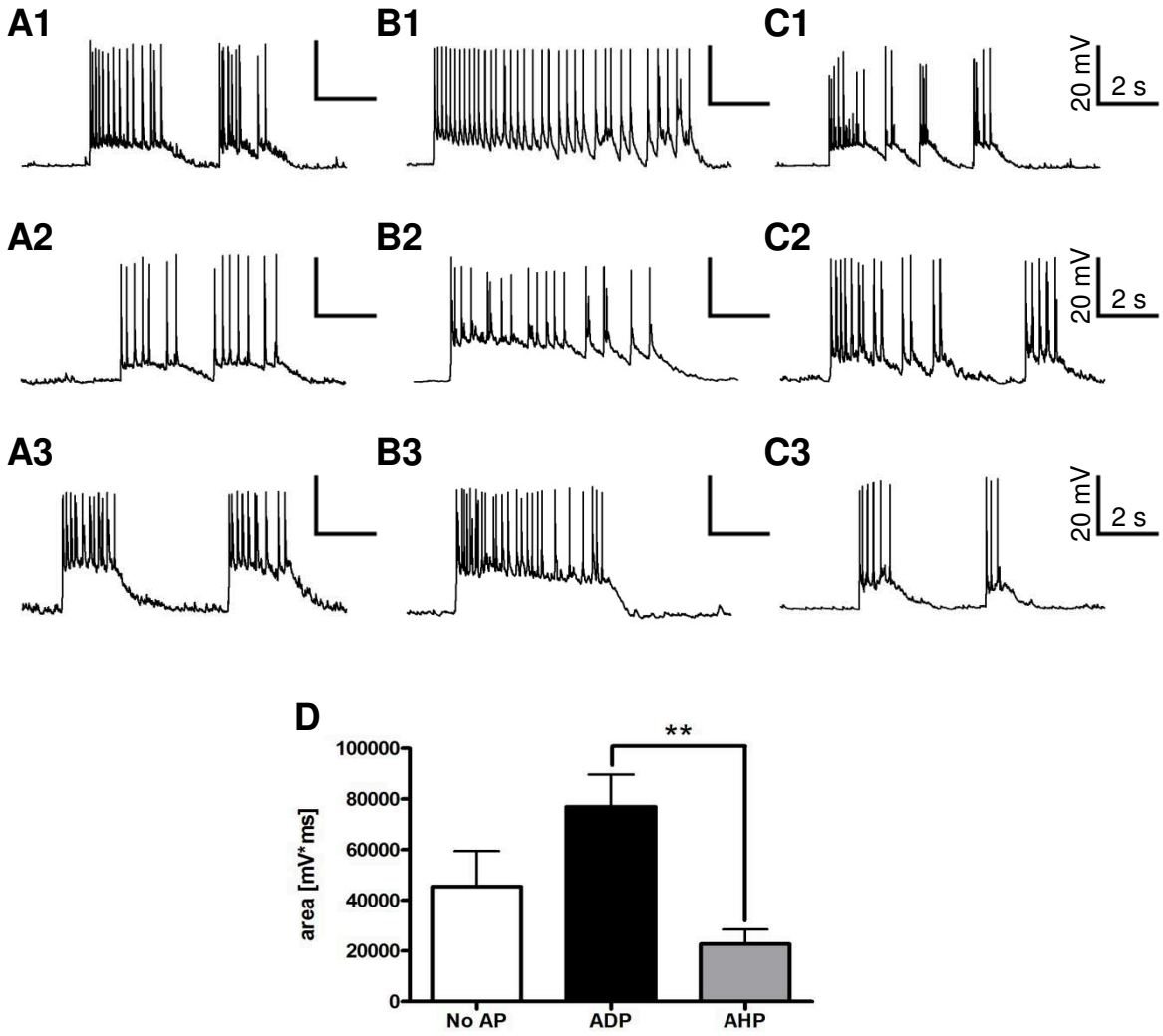

**Figure 18:** Comparison of area-below-trace (ABT) of burst events in neurons showing no distinct after-potential (No AP), ADP-generating, and AHP-generating neurons. The area of burst events (given as mV*ms) was determined via event detection operation in the presence of the LTCC agonist. A-C. 3 Sample traces of neurons lacking an after-potential (A1 - A3), in ADP-generating neurons (B1 - B3), and in cells showing an AHP (C1 - C3), all in the presence of BayK. D. Statistical analysis of recordings from neurons with no after-potential (n = 10), an ADP (n = 17), and an AHP (n = 12) reveals that depolarization waves underlying burst firing in the presence of the LTCC agonist are larger in ADP-generating neurons compared to neurons which elicit after-hyperpolarizations. No significant differences could be detected between those groups and after-potential lacking cells. Bars represent median ABTs of burst events in the three experimental groups in the presence of the LTCC agonist depicted as means ± SEM. Comparison between groups was done using Kruskal-Wallis test with Dunn's Multiple Comparison Test. ** $p < 0,01$.

## 3.4 Effect of currents underlying depolarizing or hyperpolarizing after-potentials on tonic firing

No significant differences could be detected in ABTs of spike events (Fig.19A1) and EPSPs (Fig.19A2) between the 3 experimental groups. However, a tendency towards increased spike events in ADP-generating neurons compared to neurons lacking after-potentials as well as a trend towards larger EPSPs in ADP-generating neurons compared to the other 2 experimental groups can be observed. Since IPSPs were only detected in 2 neurons with depolarizing after-potentials they were not available for statistical analysis. However, comparison between AOTs of inhibitory postsynaptic potentials between AHP-generating cells and cells lacking an after-potential did not show a significant difference (Fig.19A3).

**Figure 19:** Comparison of area-below-trace (ABT) of spike events and EPSPs as well as area-over-trace (AOT) of IPSPs in neurons with different after-potentials. A1. In the presence of BayK, ABT (given as mV*ms) of spike events does not differ between neurons lacking an after-potential (n = 11), ADP-generating neurons (n = 9), and AHP-generating neurons (n = 12). Comparison between groups was done using One-way analysis of variance and Tukey's Multiple Comparison Test ($p = 0,0615$). A2. No difference in ABT of EPSPs could be detected in neurons showing no after-potential (n = 10), an ADP (n = 8) or an AHP (n = 12) when BayK was applied. This was observed using One-way analysis of variance and Tukey's Multiple Comparison Test ($p = 0,0807$). A3. AOTs of IPSPs in the presence of BayK did not differ between neurons showing no after-potential (n = 9) and AHP-generating neurons (n = 11) which was found out with Mann Whitney test ($p = 0,7323$). AOT of IPSPs in ADP-generating cells are shown but they were excluded from this analysis since n = 2. Bars in A1 - A3 are representations of median event areas (given as mV*ms) depicted as means ± SEM. B+C. 3 sample overlay of spike events (B) and EPSPs (C) recorded in the presence of BayK from neurons lacking after-potentials (cyan), from ADP-generating neurons (black), and from AHP-generating neurons (grey) showing that in most cells no differences in size between the 3 experimental groups exist. D. 3 sample traces showing that AOT of IPSPs is not different in size between cells lacking after-potentials (cyan), ADP-generating cells (black; 2 example traces are shown), and AHP-generating cells (grey).

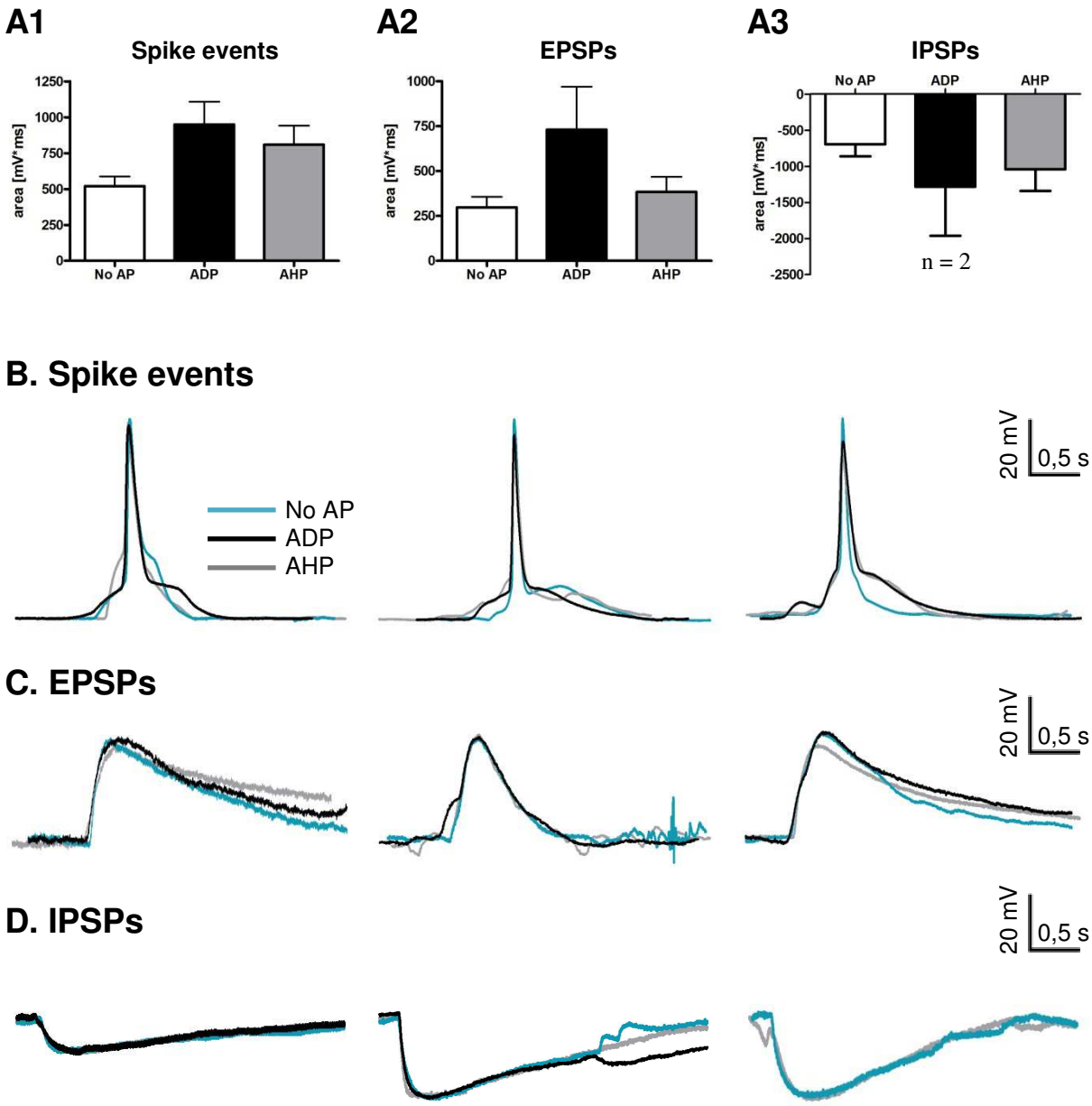


### 3.5 Dependence of burst event and action potential magnitude on after-potential area

Size of after-depolarizations evoked by brief current injections (50 ms length), at which they were most prominent, and AOT of AHPs at longest pulse durations (3 s length) were plotted against the median ABT of burst events and action potentials. No correlation between ADP magnitude and size of burst events or action potentials could be detected, and the same is true for AHPs and both firing modalities. Thus, extent of after-discharges is not a decisive factor for size of burst or spike events.

Furthermore, large ADPs can also give rise to tonic firing, whereas large AHPs can underlie the tendency of neurons to fire bursts of action potentials [Fig.20].

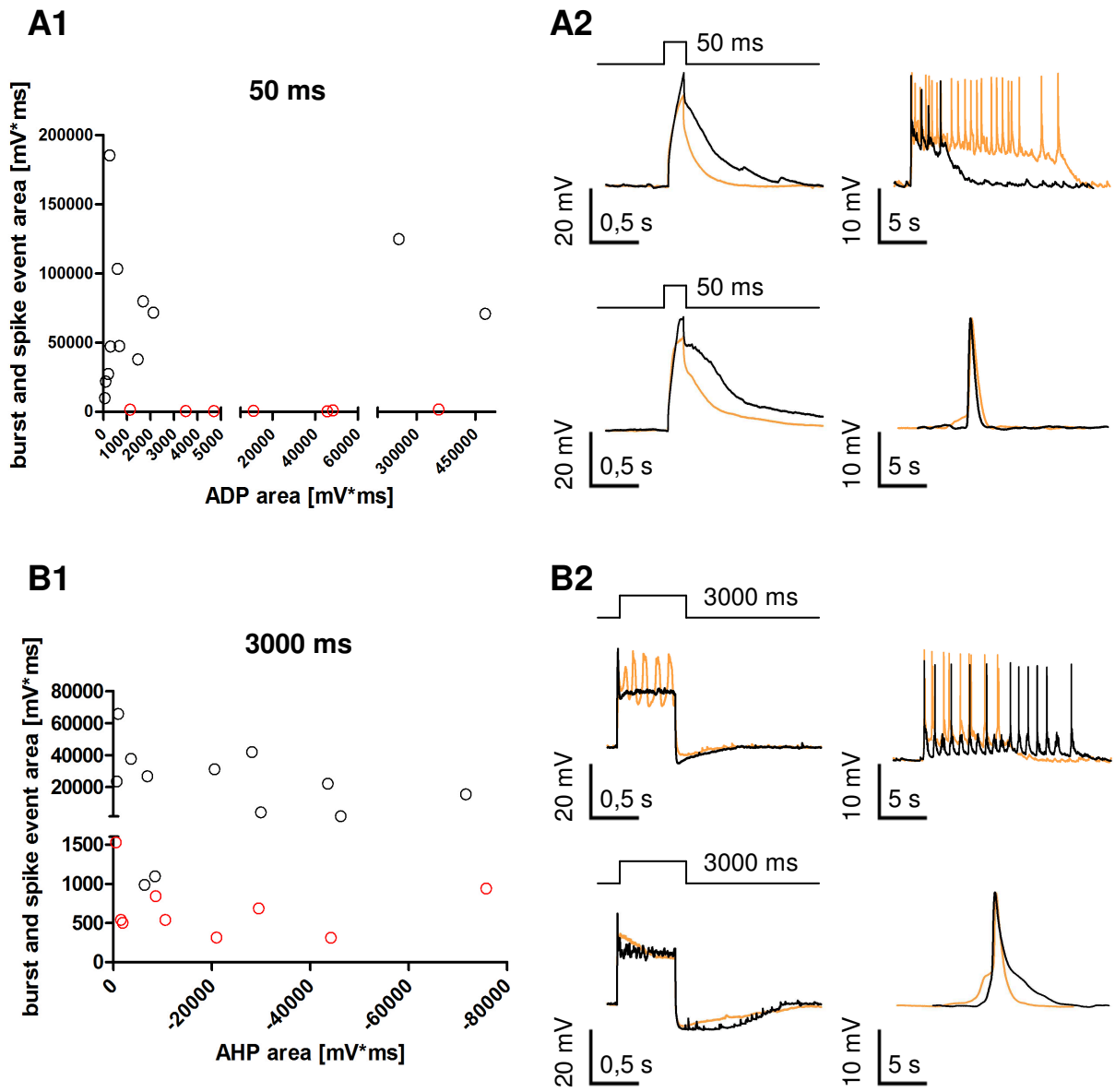


**Figure 20:** Dependence of burst and spike event area on after-potential size. A. ABT of ADPs at brief pulse durations (A1; n = 12 for bursting neurons and n = 7 for action potentials) or AOT of AHPs at long stimulus length (B1; n = 12 for bursting events and n = 9 for action potentials) was plotted against the area-below-trace of burst (black circles) and spike events (red circles). Spearman correlation analysis revealed that there is no correlation between magnitude of ADPs ($r_s$ = -0,2) or AHPs ($r_s$ = 0,1) and the extent of bursts or action potentials (all given as mV*ms). For better visualization of all data points, two gaps were inserted into the x-axis in A1 and one gap was inserted into the y-axis in B1 (To avoid overlay of data points, no gap was inserted into the y-axis in A1. However, size of spike events – red dots – in A1 was comparable to that seen in B1). A2+B2. Sample overlays of shorter (orange) and larger (black) after-depolarizations (A2) and after-hyperpolarizations (B2) and their respective firing patterns (right traces in A2 and B2).

# 4. DISCUSSION

## 4.1 Induction of tonic or burst firing is dependent on the resting membrane potential of the respective neuron

My data revealed that the occurrence of after-depolarizations or after-hyperpolarizations does not depend on the membrane potential of the respective neuron. However, tonic firing (the average Vm of these neurons amounted to -60 mV ± 6,3 mV) appeared in cells with more depolarized membrane voltages than those displaying burst firing (the average Vm of these neurons amounted to -72 mV ± 6,4 mV) [Subchapter 2.6.1, Fig.11A+B]. This is consistent with a previous finding (reviewed by Perez-Reyes, 2003). In this publication the two different firing modalities were evoked via a depolarizing stimulus and it was shown that regular (tonic) firing was yielded when the neuron was depolarized from a resting membrane potential near -55 mV, whereas burst firing was elicited with the same stimuli when the membrane voltage was more negative than -70 mV.

## 4.2 Size of after-potentials depends on the stimulus duration

ADPs or AHPs were elicited in current injection experiments when the LTCC agonist BayK was applied, but were reduced or completely eradicated in traces recorded in the presence of the LTCC antagonist isradipine. After-depolarizations were most prominent at brief current injection lengths (reaching its maximum at a current injection length of 50 ms) and decreased in size with increasing duration of the pulses, whereas after-hyperpolarizations increased with prolongation of the stimuli (reaching its maximum at a current injection length of 3 seconds) [Subchapter 2.6.2, Fig.12A-C]. Similar results have been reported in a previous study of our group (Geier et al., 2011). Furthermore, it was shown in this recent work that induction of ADPs or AHPs depends on the stimulus strength: ADPs were elicited at milder depolarizations, whereas AHPs were induced by stronger current injections.
These results suggest that excitatory and inhibitory coupling may influence electrical activity in a bimodal manner: activation of CANs may take place at brief and/ or weaker depolarizations, whereas $K_{Ca}$ channels become activated as this depolarization is prolonged and/ or becomes stronger. Via this mechanism LTCC-

CAN coupling may be involved in sustaining the depolarization wave underlying burst firing, whereas LTCC-$K_{Ca}$ coupling may participate in the termination of bursting.

### 4.3 Independency of after-potentials from age of the culture

According to several reports in the literature, after-hyperpolarizations increase with age of animals (Landfield and Pitler, 1984; Kumar and Foster, 2002; Moyer et al., 2002; Power et al., 2002; Disterhoft and Oh., 2006). It was hypothesized that these changes in the magnitude of AHPs are due to an age-dependent increase in the expression levels and/ or the distribution of neuronal LTCCs in the aging brain (Power et al., 2002; Brewer et al., 2009; Núñez-Santana et al., 2014). However, it has to be noted that these studies were carried out in hippocampal slices of young (2 to 8 month old) and aged (22 to 42 month old) rats (Landfield and Pitler, 1984; Kumar and Foster, 2002; Moyer et al., 2002; Power et al., 2002). In contrast, my experiments were done in primary culture of rat hippocampal neurons. Since it is necessary for primary culture to use cells of neonatal animals, it was not possible to distinguish between naïve and old rats. Thus, I could solely analyse if after-potentials change in their magnitude in neurons derived from neonatal rats with increasing days of culture.

Measurements of primary rat hippocampal cells were carried out starting from day 11 until day 34 after preparation and occurrence of ADPs or AHPs did not depend on the age of cells *in vitro* (Subchapter 2.6.3, Fig.13). Furthermore, magnitude of after-potentials did not increase or decrease with culture duration (Subchapter 2.6.3, Fig.14A-C). These findings demonstrate that occurrence and size of after-potentials does not change with the age of the neurons under our culture conditions. These results are further supported by the data of a previous study of our group (Geier, 2011). In this work LTCC-mediated voltage responses (bumps, oscillations, and hyperpolarizing sags) and LTCC-mediated $Ca^{2+}$ currents were compared between neurons, which were cultured starting from less than 14 days until 28 days. However, both parameters remained unaltered with increasing age of the cells *in vitro*.

### 4.4 Electrical activity of a neuron is not restricted to a distinct after-potential

According to the literature suprathreshold after-depolarizations are suggested to be the driving force of burst firing in neurons (Bean, 2007; Beck and Yaari, 2008; Brown and Randall, 2009). Additionally, application of flufenemic acid (FFA), a blocker of nonspecific cation channels (CAN), to bursting neurons converted their electrical activity into tonic firing (Mrejeru et al., 2011). Contrary effects could be detected upon pharmacological modulation of $Ca^{2+}$-dependent potassium channels ($K_{Ca}$, probably SK channels), which are suggested to be the driving force of after-hyperpolarizations. Hence, apamin, an antagonist of these channels induced bursts, whereas potentiation of these channels (via 1-EBIO) restricted neuronal activity to a tonic firing pattern (Stocker, 2004).

In a previous study of our group (Geier et al., 2011) it was described that rat hippocampal neurons can be distinguished according to their preferential coupling to one of these calcium-dependent conductances: in some neurons $Ca^{2+}$-Influx via LTCCs is coupled predominantly to CAN channels, mediating ADPs, whereas in others activation of $Ca^{2+}$-dependent potassium channels prevails and results in the generation of AHPs. This finding allowed me to investigate the role of after-discharges in the electrical activity of rat hippocampal cells with a different approach than those described in literature. Thus, I first recorded the firing pattern of a neuron under application of the LTCC agonist and then employed current injections in the presence of the action potential blocker tetrodotoxin (TTX) and the LTCC agonist BayK in order to determine if the respective neuron is either prone to excitatory or inhibitory coupling.

In this way I found out that both, ADP- and AHP-generating cells, are capable of discharging in a tonic or burst firing pattern. This was also true for neurons that did not show any distinct after-potential upon current injection in the presence of BayK. However, in cells prone to generation of after-depolarizations, bursting was discovered more often as regular firing, whereas similar distribution of these firing patterns could be observed between the other two experimental groups (Subchapter 3.1, Table 2, Fig.16). Taken together, neither LTCC-CAN coupling nor LTCC-$K_{Ca}$ coupling seem to be a decisive factor for the generation of these specific firing behaviours. Induction of tonic or burst firing may rather depend on the membrane voltage, the network activity and/ or the expression levels of distinct ion channels of the respective neuron. Hence, the discrepancies in the distribution of regular firing

and bursting, observed in cells prone to ADP-generation, rather rely on the intrinsic properties of these cells other than the LTCC-CAN coupling.

### 4.5 LTCC-mediated active voltage responses in neurons with different after-potentials

In accordance to the findings of a previous study of our group (Geier et al., 2011) bumps predominated in ADP-generating neurons, whereas hyperpolarizing sags made up the vast majority of LTCC-mediated active voltage responses in AHP-generating neurons. Furthermore, in most of the cells which did not elicit a distinct after-potential, no active voltage responses could be observed. Oscillations were detected in neurons which elicited after-hyperpolarizations and in neurons lacking an after-potential, but were not seen in those neurons showing after-depolarizations (Subchapter 3.2, Table 3, Fig.17). An explanation for this lack of oscillations in ADP-generating neurons might come from two of our recent studies (Goldnagl, 2012; Hasreiter, 2012). These works focused on the role of $Ca_V1.2$ and $Ca_V1.3$ in the excitability of central neurons. Hence, two knockout models of primary mice hippocampal neurons were employed in these studies: a pharmacological knockout of $Ca_V1.2$, which exhibits lower sensitivity to DHPs ($Ca_V1.2$ $DHP^{-/-}$) and a $Ca_V1.3$ knockout ($Ca_V1.3^{-/-}$). Pulse injection experiments in the presence of BayK were carried out to evoke after-potentials and LTCC-mediated active voltage responses (bumps, oscillations, and hyperpolarizing sags). AHPs could be observed in both knockout models, whereas ADPs were solely elicited in $Ca_V1.3^{-/-}$ neurons. This suggests that coupling of $Ca^{2+}$-Influx through $Ca_V1.2$ to CANs alone is responsible for induction of after-depolarizations, whereas both isoforms are involved in the generation of hyperpolarizing after-potentials. Additionally, oscillations were missing in both knockout models but were detected in wild-type mice, indicating that $Ca_V1.2$ and $Ca_V1.3$ together are necessary to generate oscillatory voltage responses. Thus, activation of CANs via $Ca^{2+}$-Influx through $Ca_V1.2$ may underlie ADP-generation, and since $Ca_V1.3$ seems to be not involved in this process, oscillations may be missing in neurons showing depolarizing after-potentials. On the other hand both isoforms may be necessary for the generation of AHPs and this may be the reason for the occurrence of oscillations in cells eliciting hyperpolarizing after-potentials.

## 4.6 Currents underlying different after-potentials are involved in the modulation of burst firing

It has been hypothesized in the literature that nonspecific cation channels (CAN; possibly TRPM4b or TRPM5) may be involved in the induction of burst firing and/ or in the prolongation of the burst plateau phase (Beurrier et al., 1999; Morrisset and Nagy, 1999; Pape et al., 2004; Lee and Tepper, 2007; Mrejeru et al., 2011; Pressler and Regehr, 2013). On the other hand, it was postulated that $Ca^{2+}$-activated $K^+$ conductances ($K_{Ca}$; probably SK channels) may contribute to burst termination (Beurrier et al., 1999; Kitai et al., 1999; Hallworth et al., 2003; Pape et al., 2004; Stocker, 2004; Kim and Trussell, 2007; Cain and Snutch, 2010; Mrejeru et al., 2011). Indeed, coupling of $Ca^{2+}$-Influx through LTCCs to CAN (ADP-generating neurons) led to an augmentation of depolarization waves underlying burst firing, whereas those events were significantly smaller in neurons prone to LTCC-$K_{Ca}$ coupling (AHP-generating neurons). Furthermore, ABT of burst events did not differ significantly between those cells that did not give rise to a distinct after-potential and the other two experimental groups, although a tendency towards decreased or increased size of burst events could be detected compared to neurons prone to excitatory coupling or neurons prone to inhibitory coupling, respectively (Subchapter 3.3; Fig.18A-D). Together these results demonstrate that the currents underlying ADP-generation or AHP-generation play a pivotal role in the modulation of burst firing.

## 4.7 Currents underlying different after-potentials are not involved in the modulation of spike events, EPSPs and IPSPs

The magnitude of spike events did not significantly differ between the 3 experimental groups investigated in this study (Subchapter 3.4; Fig.19A1+B). It has been described in the literature that LTCCs only have a negligible impact on the modulation of action potentials and, since they have slower activation kinetics than sodium channels, may rather play a role during the falling phase than during the rising phase of spike events (Helton et al., 2005; Bean, 2007; Lacinova et al., 2008). However, a tendency towards smaller spike events in neurons, which did not give rise to a distinct after-potential, compared to ADP- and AHP-generating neurons

could be observed in my recordings (Subchapter 3.4; Fig.19A1 and right example in B).

Furthermore, no differences in the size of excitatory postsynaptic potentials could be detected between the 3 experimental groups, although a tendency towards increased ABTs of EPSPs was seen in ADP-generating neurons compared to AHP-generating neurons (Subchapter 3.4; Fig.19A2+C). Additionally, statistical comparison of AOT of IPSPs revealed that magnitude of these events did not differ between AHP-generating cells and cells lacking a distinct after-potential (Subchapter 3.4; Fig.13A3+D). Neurons eliciting a depolarizing after-potential were not available for this analysis, since inhibitory postsynaptic potentials were only observed in two neurons of this group. However, overlays of IPSP samples from these two ADP-generating cells with samples of such events from AHP-generating and after-potential lacking cells, suggest that magnitude of IPSPs may not differ between the 3 experimental groups (Subchapter 3.4; left and middle samples in Fig.19D).

### 4.8 Magnitude of after-potentials does not correlate with the size of spike and/ or burst events

Correlation analysis indicated that the magnitude of after-potentials does not have an impact on the size of single action potentials or bursts. This means that both, larger or smaller after-depolarizations, are capable of generating small or large spike or burst events and the same is true for after-hyperpolarizations (Subchapter 3.5, Fig.20A1-B2). However, it has to be noted that current-injection induced depolarizations were used in my experiments to depolarize the membrane to the activation threshold of LTCCs and to induce after-potentials in the presence of BayK. Hence, I cannot rule out the possibility that the magnitude of depolarizing or hyperpolarizing after-potentials, induced by endogenously evoked depolarizations, may have an influence on the size of spike and/ or burst events.

After-potentials are thought to be decaying representations of conductances underlying LTCC-mediated active voltage responses (bumps, hyperpolarizing sags, oscillations) evoked by current injections in the presence of BayK. Hence, the different voltage response modes may modulate spike events and/ or bursts in a contrary way. LTCC-CAN coupling seems to underlie the generation of bumps and its depolarizing effect on the membrane may lead to an augmentation of action

potentials and/ or bursting. In contrast, hyperpolarizing sags, mediated via LTCC-$K_{Ca}$ coupling, may reduce these events through membrane hyperpolarization. This is particularly imaginable since both voltage responses were observed in ADP- and AHP-generating neurons. However, further experiments will be necessary to shed light on this hypothesis.

# 5. CONCLUSION

This study on primary hippocampal neurons reports that coupling of $Ca^{2+}$-Influx through L-type voltage-gated calcium channels (LTCCs) to either nonspecific cation channels (CAN) or calcium-dependent $K^+$ channels ($K_{Ca}$) plays a pivotal role in the modulation of hippocampal firing patterns, since burst events were significantly augmented in neurons with predominant LTCC-CAN coupling compared to neurons prone to LTCC-$K_{Ca}$ coupling. Contrary, spike events, excitatory postsynaptic potentials (EPSPs), and inhibitory postsynaptic potentials (IPSPs) were not influenced by the distinct LTCC-coupling modes. Additionally, magnitude of spike and/ or burst events did not correlate with the size of after-potentials in my recordings. Furthermore, it was shown that LTCC-CAN or LTCC-$K_{Ca}$ coupling is not a decisive factor for the generation of a specific neuronal firing modality but that induction of tonic or burst firing may rather depend on the membrane potential, the network activity and/ or the ion channel composition of the respective cell.

# 6. REFERENCES


Alexander SPH., Mathie A., Peters JA. (2011) Guide to Receptors and Channels (GRAC), 5th edn. British Journal of Pharmacology 164(Suppl.1):S1-S324.

Andrade R., Foehring RC., Tzingounis AV. (2012) The calcium-activated slow AHP: cutting through the Gordian knot. Frontiers in Cellular Neuroscience 6:1-12.

Baumann L., Gerstner A., Zong X., Biel M., Wahl-Schott C. (2004) Functional Characterization of the L-type $Ca^{2+}$ Channel $Ca_v1.4\alpha1$ from Mouse Retina. Investigative Ophthalmology & Visual Science 45:708-713.

Bean BP. (2007) The action potential in mammalian central neurons. Nature Reviews Neuroscience 8:451-465.

Beck H. and Yaari Y. (2008) Plasticity of intrinsic neuronal properties in CNS disorders. Nature Reviews Neuroscience 9:357-369.

Berridge MJ. (2012) Ion Channels. Cell Signalling Biology, Module 3:3.1-3.72.

Beurrier C., Congar P., Bioulac B., Hammond C. (1999) Subthalamic Nucleus Neurons Switch from Single-Spike Activity to Burst-Firing Mode. The Journal of Neuroscience 19:599-609.

Brewer LD., Dowling ALS., Curran-Rauhut MA., Landfield PW., Porter NM., Blalock EM. (2009) Estradiol Reverses a Calcium-Related Biomarker of Brain Aging in Female Rats. The Journal of Neuroscience 29:6058-6067.

Brown JT. and Randall AD. (2009) Activity-dependent depression of the spike after-depolarization generates long-lasting intrinsic plasticity in hippocampal CA3 pyramidal neurons. The Journal of Physiology 587.6:1265-1281.

Cain SM. and Snutch TP. (2010) Contributions of T-type calcium channel isoforms to neuronal firing. Channels 4:475-482.

Calin-Jageman I. and Lee A. (2008) $Ca_v1$ L-type $Ca^{2+}$ channel signalling complexes in neurons. Journal of Neurochemistry 105:573-583.

Catterall WA., Perez-Reyes E., Snuth TP., Striessnig J. (2005) International Union of Pharmacology. XLVIII. Nomenclature and Structure-Function Relationship of Voltage-Gated Calcium Channels. Pharmacological Reviews 57:411-425.

Catterall WA. (2011) Voltage-Gated Calcium Channels. Cold Spring Harbor Perspectives in Biology 3:1-23.

Cha A., Snyder GE., Selvin PR., Bezanilla F. (1999) Atomic scale movement of the voltage-sensing region in a potassium channel measured via spectroscopy. Nature 402:809-813.

Chen QH. and Toney GM. (2009) Excitability of paraventricular nucleus neurones that project to the rostral ventrolateral medulla is regulated by small-conductance $Ca^{2+}$-activated $K^+$ channels. The Journal of Physiology 587.17:4235-4247.

Cingolani LA., Gymnopoulos M., Boccaccio A., Stocker M., Pedarzani P. (2002) Developmental Regulation of Small-Conductance Ca2+-Activated K+ Channel Expression and Function in Rat Purkinje Neurons. The Journal of Neuroscience 22:4456-4467.

Clark NC., Nagano N., Kuenzi FM., Jarolimek W., Huber I., Walter D., Wietzorrek G., Boyce S., Kullmann DM., Striessnig J., Seabrook GR. (2003) Neurological phenotype and synaptic function in mice lacking the $Ca_v1.3$ α subunit of neuronal L-type voltage-dependent $Ca^{2+}$ channels. Neuroscience 120:435-442.

Disterhoft JF. and Oh MM. (2006) Learning, aging and intrinsic neuronal plasticity. Trends in Neurosciences 29:587-599.

Dolphin AC. (2009) Calcium channel diversity: multiple roles of calcium channel subunits. Current Opinion in Neurobiology 19:237-244.

Dolphin AC. (2012) Calcium channel auxiliary $\alpha_2\delta$ and $\beta$ subunits: trafficking and one step beyond. Nature Reviews Neuroscience 13:542-555.

Elmslie K. (2004) Calcium Channel Blockers in the Treatment of Disease. Journal of Neuroscience Research 75:733-741.

Ertel EA., Campbell KP., Harpold MM., Hofmann F., Mori Y., Perez-Reyes E., Schwartz A., Snutch TP., Tanabe T., Birnbaumer L., Tsien RW., Catterall WA. (2000) Nomenclature of Voltage-Gated Calcium Channels. Neuron 25:533-535.

Flucher BE. and Franzini-Armstrong C. (1996) Formation of junctions involved in excitation-contraction coupling in skeletal and cardiac muscle. Proceedings of the National Academy of Sciences 93:8101-8106.

Fox AP., Nowycky MC., Tsien RW. (1987) Kinetic and pharmacological properties distinguishing three types of calcium currents in chick sensory neurones. The Journal of Physiology 394:149-172.

Gamelli AE., McKinney BC., White JA., Murphy GG. (2011) Deletion of the L-Type Calcium Channel Cav1.3 but not Cav1.2 Results in a Diminished sAHP in Mouse CA1 Pyramidal Neurons. Hippocampus 21:133-141.

Geier P. (2011) Modulation of neuronal excitability via L-type calcium channel mediated coupling modes [PhD Thesis]. Medical University of Vienna [unpublished data].

Geier P., Lagler M., Boehm S., Kubista H. (2011) Dynamic interplay of excitatory and inhibitory coupling modes of neuronal L-type calcium channels. The American Journal of Physiology – Cell Physiology 300:C937-C949.

Goldnagl L. (2012) The role of $Ca_V1.3$ L-type calcium channels in the excitability of central neurons [Bachelor Thesis]. University of Veterinary Medicine Vienna [unpublished data].

Gu N., Veryaeke K., Hu H., Storm JF. (2005) Kv7/KCNQ/M and HCN/h, but not $K_{Ca}2$/SK channels, contribute to the somatic medium after-hyperpolarization and excitability control in CA1 hippocampal pyramidal cells. The Journal of Physiology 566.3:689-715.

Hallworth NE., Wilson CJ., Bevan MD. (2003) Apamin-Sensitive Small Conductance Calcium-Activated Potassium Channels, through their Selective Coupling to Voltage-Gated Calcium Channels, Are Critical Determinants of the Precision, Pace, and Pattern of Action Potential Generation in Rat Subthalamic Nucleus Neurons *In Vitro*. The Journal of Neuroscience 23:7525-7542.

Hasreiter J. (2012) The role of $Ca_V1.2$ L-type calcium channels in the excitability of central neurons [Bachelor thesis]. University of Veterinary Medicine Vienna [unpublished data].

Helton TD., Xu W., Lipscombe D. (2005) Neuronal L-Type Calcium Channels Open Quickly and Are Inhibited Slowly. The Journal of Neuroscience 25:10247-10251.

Herman JP., Chen KC., Booze R., Landfield PW. (1998) Up-Regulation of $\alpha_{1D}$ $Ca^{2+}$ Channel Subunit mRNA Expression in the Hippocampus of Aged F344 Rats. Neurobiology of Aging 19:581-587.

Hille B. ($2001^3$) Ion Channels of Excitable Membranes. Sunderland, MA, U.S.A.: Sinauer Associates, Inc.

Hofmann T., Chubanov V., Gudermann T., Montell C. (2003) TRPM5 Is a Voltage-Modulated and $Ca^{2+}$-Activated Monovalent Selective Cation Channel. Current Biology 13:1153-1158.

Hofmann ME. and Frazier CJ. (2010) Muscarinic receptor activation modulates the excitability of hilar mossy cells through the induction of an afterdepolarization. Brain Research 1318:42-51.

Horn R. and Marty A. (1988) Muscarinic Activation of Ionic Currents Measured by a New Whole-Cell Recording Method. The Journal of General Physiology 92:145-149.

Kim Y. and Trussell LO. (2007) Ion Channels Generating Complex Spikes in Cartwheel Cells of the Dorsal Cochlear Nucleus. Journal of Neurophysiology 97:1705-1725.

Kitai ST., Shepard PD., Callaway JC., Scroggs R. (1999) Afferent modulation of dopamine neuron firing patterns. Current Opinion in Neurobiology 9:690-697.

Kochegarov AA. (2003) Pharmacological modulators of voltage-gated calcium channels and their therapeutical application. Cell Calcium 33:145-162.

Koschak A., Reimer D., Huber I., Grabner M., Glossmann H., Engel J., Striessnig J. (2001) α1D (Cav1.3) Subunits Can Form L-type $Ca^{2+}$ Channels Activating at Negative Voltages. The Journal of Biological Chemistry 276:22100-22106.

Kumar A. and Foster TC. (2002) 17β-Estradiol Benzoate Decreases the AHP Amplitude in CA1 Pyramidal Neurons. Journal of Neurophysiology 88:621-626.

Lacinova L., Moosmang S., Langwieser N., Hofmann F., Kleppisch T. (2008) $Ca_V1.2$ calcium channels modulate the spiking pattern of hippocampal pyramidal cells. Life Sciences 82:41-49.

Lai HC. and Jan LY. (2006) The distribution and targeting of neuronal voltage-gated ion channels. Nature Reviews Neuroscience 7:548-562.

Landfield PW. and Pitler TA. (1984) Prolonged $Ca^{2+}$-Dependent

Afterhyperpolarizations in Hippocampal Neurons of Aged Rats. Science 226:1089-1092.

Launay P., Fleig A., Perraud AL., Scharenberg AM., Penner R., Kinet JP. (2002) TRPM4 Is a $Ca^{2+}$-Activated Nonselective Cation Channel Mediating Cell Membrane Depolarization. Cell 109:397-407.

Lee CR. and Tepper JM. (2007) A Calcium-Activated Nonselective Cation Conductance Underlies the Plateau Potential in Rat Substantia Nigra GABAergic Neurons. The Journal of Neuroscience 27:6531-6541.

Lipscombe D., Pan JQ., Gray AC. (2002) Functional Diversity in Neuronal Voltage-Gated Calcium Channels by Alternative Splicing of $Ca_V\alpha_1$. Molecular Neurobiology 26:21-44.

Lipscombe D., Helton TD., Xu W. (2004) L-Type Calcium Channels: The Low Down. Journal of Neurophysiology 92:2633-2641.

Lisman JE. (1997) Bursts as units of neural information: making unreliable synapses reliable. Trends in Neurosciences 20:38-43.

Liu X. and Herbison AE. (2008) Small-Conductance Calcium-Activated Potassium Channels Control Excitability and Firing Dynamics in Gonadotropin-Releasing Hormone (GnRH) Neurons. Endocrinology 149:3598-3604.

Llinás R., Sugimori M., Lin JW., Cherksey B. (1989) Blocking and isolation of a calcium channel from neurons in mammals and cephalopods utilizing a toxin fraction (FTX) from funnel-web spider poison. Proceedings of the National Academy of Sciences 86:1689-1693.

Ludwig A., Flockerzi V., Hofmann F. (1997) Regional Expression and Cellular Localization of the α1 and β Subunit of High Voltage-Activated Calcium Channels in Rat Brain. The Journal of Neuroscience 17:1339-1349.

McRory JE., Hamid J., Doering CJ., Garcia E., Parker R., Hamming K., Chen L., Hildebrand M., Beedle AM., Feldcamp L., Zamponi GW., Snutch TP. (2004) The *CACNA1F* Gene Encodes an L-Type Calcium Channel with Unique Biophysical Properties and Tissue Distribution. The Journal of Neuroscience 24:1707-1718.

Molleman A. (2003) Patch clamping: an introductory guide to patch clamp electrophysiology. The Atrium, Southern Gate, Chichester, West Sussex, England: John Wiley & Sons, Ltd.

Moosmang S., Haider N., Klugbauer N., Adelsberger H., Langwieser N., Müller J., Stiess M., Marais E., Schulla V., Lacinova L., Goebbels S., Nave KA., Storm DR., Hofmann F., Kleppisch T. (2005) Role of Hippocampal Cav1.2 Ca2+ Channels in NMDA Receptor-Independent Synaptic Plasticity and Spatial Memory. The Journal of Neuroscience 25:9883-9892.

Morisset V. and Nagy F. (1999) Ionic Basis for Plateau Potentials in Deep Dorsal Horn Neurons of the Rat Spinal Cord. The Journal of Neuroscience 19:7309-7316.

Moyer JR., Power JM., Thompson LT., Disterhoft JF. (2002) Increased Excitability of Aged Rabbit CA1 Neurons after Trace Eyeblink Conditioning. The Journal of Neuroscience 20:5476-5482.

Mrejeru A., Wei A., Ramirez JM. (2011) Calcium-activated non-selective cation currents are involved in generation of tonic and bursting activity in dopamine neurons of the substantia nigra pars compacta. The Journal of Physiology 589.10:2497-2514.

Nilius B., Prenen J., Tang J., Wang C., Owsianik G., Janssens A., Voets T., Zhu MX. (2005) Regulation of the $Ca^{2+}$-Sensitivity of the Nonselective Cation Channel TRPM4. The Journal of Biological Chemistry 280:6423-6433.

Nowycky MC., Fox AP., Tsien RW. (1985a) Long-opening mode of gating of neuronal

calcium channels and its promotion by the dihydropyridine calcium agonist Bay K 8644. Proceedings of the National Academy of Sciences 82:2178-2182.

Nowycky MC., Fox AP., Tsien RW. (1985b) Three types of neuronal calcium channel with different calcium agonist sensitivity. Nature 316:440-443.

Numberger M. and Draguhn A. (1996) Patch-Clamp Technik. Heidelberg, Berlin, Oxford: Spektrum Akademischer Verlag.

Núñez-Santana FL., Oh MM., Antion MD., Lee A., Hell JW., Disterhoft JF. (2014) Surface L-type Ca2+ channel expression levels are increased in aged hippocampus. Aging Cell 13:111-120.

Okada Y. (2012) Patch Clamp Techniques: From Beginning to Advanced Protocols. Tokyo, Dordrecht, Heidelberg, London, New York: Springer.

Overton PG. and Clark D. (1997) Burst firing in midbrain dopaminergic neurons. Brain Research Reviews 25:312-334.

Pape HC., Munsch T., Budde T. (2004) Novel vistas of calcium-mediated signalling in the thalamus. Pflügers Archiv – European Journal of Physiology 448:131-138.

Perez-Reyes E. (2003) Molecular Physiology of Low-Voltage-Activated T-type Calcium Channels. Physiological Reviews 83:117-161.

Power JM., Wu WW., Sametsky E., Oh MM., Disterhoft JF. (2002) Age-Related Enhancement of the Slow Outward Calcium-Activated Potassium Current in Hippocampal CA1 Pyramidal Neurons In Vitro. The Journal of Neuroscience 22:7234-7243.

Pressler RT. and Regehr WG. (2013) Metabotropic Glutamate Receptors Drive Global Persistent Inhibition in the Visual Thalamus. The Journal of Neuroscience 33:2494-2506.

Sherman-Gold R. (2006[2]) The Axon CNS Guide to Electrophysiology & Biophysics Laboratory Techniques. Molecular Devices Corporation.

Smith RS. and Araneda RC. (2010) Cholinergic Modulation of Neuronal Excitability in the Accessory Olfactory Bulb. Journal of Neurophysiology 104:2963-2974.

Stocker M. (2004) $Ca^{2+}$-activated $K^{+}$ channels: molecular determinants and function of the SK family. Nature Reviews Neuroscience 5:758-770.

Teruyama R. and Armstrong WE. (2007) Calcium-Dependent Fast Depolarizing Afterpotentials in Vasopressin Neurons in the Rat Supraoptic Nucleus. Journal of Neurophysiology 98:2612-2621.

Tippens AL., Pare JF., Langwieser N., Moosmang S., Milner TA., Smith Y., Lee A. (2008) Ultrastructural Evidence for Pre- and Postsynaptic Localization of $Ca_v1.2$ L-Type $Ca^{2+}$ Channels in the Rat Hippocampus. The Journal of Comparative Neurology 506:569-583.

Triggle DJ. (2003) 1,4-Dihydropyridines as Calcium Channel Ligands and Privileged Structures. Cellular and Molecular Neurobiology 23:293-303.

Trimmer JS. and Rhodes KJ. (2004) Localization of voltage-gated ion channels in mammalian brain. Annual Review of Physiology 66:477-519.

Ullrich ND., Voets T., Prenen J., Vennekens R., Talavera K., Droogmans G., Nilius B. (2005) Comparison of functional properties of the $Ca^{2+}$-activated cation channels TRPM4 and TRPM5 from mice. Cell Calcium 37:267-278.

Xu W. and Lipscombe D. (2001) Neuronal $Ca_{v1.3\alpha1}$ L-Type Channels Activate at Relatively Hyperpolarized Membrane Potentials and Are Incompletely Inhibited by Dihydropyridines. The Journal of Neuroscience 21:5944-5951.

Zhang W. and Linden DJ. (2003) The other side of the engram: Experience-driven

changes in neuronal intrinsic excitability. Nature Reviews Neuroscience 4:885-900.

Zhao Y., Inayat S., Dikin DA., Singer JH., Ruoff RS., Troy JB (2009) Patch clamp technique: review of the current state of the art and potential contributions from nanoengineering. Journal of Nanoengineering and Nanosystems: Proceedings of the Institution of Mechanical Engineers Part N 222:1-11.

„Ich habe mich bemüht, sämtliche Inhaber der Bildrechte ausfindig zu machen und ihre Zustimmung zur Verwendung der Bilder in dieser Arbeit eingeholt. Sollte dennoch eine Urheberrechtsverletzung bekannt werden, ersuche ich um Meldung bei mir."

# 7. ABBREVIATIONS

| | |
|---|---|
| A | amplifier |
| ABT | area-below-trace |
| ADP | after-depolarization |
| AHP | after-hyperpolarization |
| AID | alpha-interaction domain |
| ANOVA | Analysis of variance |
| AOT | area-over-trace |
| ARA-C | Cytosin-β-D-arabinofuranosid hydrochloride |
| AT | application tip |
| ATP | adenosine triphosphate |
| BayK | Bay K 8644 |
| BK | big conductance |
| BTZ | benzothiazepine |
| °C | degree Celsius |
| $[Ca^{2+}]_i$ | internal free calcium |
| CA | cornu ammonis |
| CAN | nonspecific cation channel |
| CC | current clamp |
| $C_m$ | membrane capacitance |
| CS | conditioned stimulus |
| d | day |
| DA | differential amplifier |
| DAD | superfusion system |
| DG | dentate gyrus |
| DHP | dihydropyridine |
| DIGI | digitizer |
| D-MEM | Dulbecco's Modified Eagle Medium |
| DMSO | dimethyl sulfoxide |
| EPSP | excitatory postsynaptic potential |
| fAHP | fast after-hyperpolarization |
| FC | Faraday cage |
| FCS | fetal calf serum |

| | |
|---|---|
| FFA | flufenemic acid |
| g | gram |
| HVA | high-voltage-activated |
| Hz | Hertz |
| I | current |
| $I_c$ | compensatory current |
| $I_{CAN}$ | nonspecific cation channel current |
| $I_{in}$ | injected current |
| $I_{K,Ca}$ | $Ca^{2+}$-dependent $K^+$ channel current |
| $I_L$ | L-type $Ca^{2+}$ current |
| IPSP | inhibitory postsynaptic potential |
| ISH | In situ hybridization |
| isr | isradipine |
| ITS | insulin:transferrin:Na-selenite |
| kDA | kilodalton |
| $K_{Ca}$ | $Ca^{2+}$-dependent potassium channel |
| $K_v$ | voltage-gated potassium channel |
| l | litre |
| LTCC | L-type voltage-gated calcium channel |
| LTS | low threshold calcium spikes |
| LVA | low-voltage-activated |
| M | microscope table |
| mAHP | medium after-hyperpolarization |
| ME | microelectrode |
| µl | microlitre |
| µm | micromolar |
| mg | milligram |
| ml | millilitre |
| mm | millimetre |
| mM | millimolar |
| MΩ | MegaOhm |
| ms | millisecond |
| mV | millivolt |
| MVA | medium-voltage-activated |

| | |
|---|---|
| N | neuron |
| n.A. | not available |
| nM | nanomolar |
| No AP | No after-potential |
| NTCC | N-type voltage-gated calcium channel |
| NUTS | nutrients |
| OA | operational amplifier |
| p-loop | pore loop |
| Pa | Pascal |
| pA | picoampere |
| PA | preamplifier |
| PAA | phenylalkylamine |
| PC | personal computer |
| PDL | Poly-D-Lysine |
| PP | patch pipette |
| PtdIns(4,5)$P_2$ | Phosphatidylinositol 4,5-biphosphate |
| PTCC/ QTCC | P-type/ Q-type voltage-gated calcium channel |
| R | resistance |
| $R_a$ | access resistance |
| RE | reference (bathing) electrode |
| $R_f$ | feedback resistance |
| $R_m$ | membrane resistance |
| $R_p$ | pipette resistance |
| RTCC | R-type voltage-gated calcium channel |
| RyR1 | type 1 ryanodine-sensitive $Ca^{2+}$ release channel |
| s | second |
| S | superfusion device |
| SA | summing amplifier |
| sAHP | slow after-hyperpolarization |
| SEM | standard error of the mean |
| SK | small conductance |
| TMC | anti-vibrating table |
| TRPM | melastatin-related subfamily of transient receptor potential channels |

| | |
|---|---|
| TTCC | T-type voltage-gated calcium channel |
| TTX | tetrodotoxin |
| U | Unit |
| US | unconditioned stimulus |
| VC | voltage clamp |
| $V_{cmd}$, $U_o$ | command (holding) potential |
| VGCC | Voltage-gated calcium channel |
| VGKC | Voltage-gated potassium channel |
| VGSC | Voltage-gated sodium channel |
| Vm | membrane voltage |
| $V_p$ | pipette voltage |

# 8. APPENDIX

## 8.1 Abstract

It has long been known that $Ca^{2+}$-dependent conductances play a crucial role in the regulation of neuronal discharge activity. For example, the $Ca^{2+}$-dependent nonspecific cation channel (CAN)-mediated ion current ($I_{CAN}$) is thought to underlie the tendency of neurons to fire bursts of action potentials, whereas the $Ca^{2+}$-dependent $K^+$-channel ($K_{Ca}$)-mediated current ($I_{K,Ca}$) has been strongly linked to tonic firing patterns. In a previous study of our group rat hippocampal neurons were shown to be distinguishable according to their preferential L-type voltage-gated calcium channel (LTCC) coupling. The distinction was particularly evident when tetrodotoxin (TTX) was used to block neuronal firing and when LTCC activity was potentiated by BayK. Then a preferential coupling of LTCC-mediated $Ca^{2+}$-Influx to CAN channels gave rise to after-depolarizations (ADPs), as soon as the current injection was switched off, because $I_{CAN}$ outlasts the artificial depolarization. In contrast, a preferential coupling to $K_{Ca}$ channels gave rise to after-hyperpolarizations (AHPs), as $I_{K,Ca}$ is still active after the current-induced depolarization. The aim of my study was to test the above-mentioned functional excitatory links by determination of the preferential LTCC-coupling together with registration of the discharge activity that predominates in the presence of the LTCC agonist.

Neuronal electrical activity was recorded in current-clamp mode with the minimally invasive perforated-patch method. Discharge activity was quantified by determination of area-below-trace (ABT). Predominating L-type calcium channel-coupling in the respective neurons then was identified via current-injection-induced depolarizations in the presence of TTX. LTCC-activity was modulated using BayK and the LTCC antagonist isradipine.

My data demonstrate that induction of burst or tonic firing is not dependent on LTCC-CAN coupling and LTCC-$K_{Ca}$ coupling, since both firing modalities were observed in ADP- and in AHP-generating neurons. Additionally, I gained evidence that induction of these discharge activities rather depends on the membrane potential of the respective cell, as hyperpolarized membrane voltages are required to evoke burst firing and more depolarized membrane voltages favour tonic firing. Furthermore, LTCC-CAN coupling was evoked with shorter depolarizations, indicating a possible

role in burst initiation and/ or in the burst plateau phase, whereas LTCC-$K_{Ca}$ coupling predominated when current injections were longer-lasting, suggesting an involvement in burst termination. Indeed, the first coupling mode augmented burst events compared to neurons in which the latter coupling mode was predominating. Conversely, smaller events (spike events, excitatory and inhibitory postsynaptic potentials) remained unaltered between those two experimental groups. Furthermore, the size of after-potentials did not correlate with the extent of burst or spike events in my recordings. Hence, my data suggest that LTCC-induced $I_{CAN}$ and $I_{K,Ca}$ have no decisive, but rather a modulatory role in hippocampal firing patterns.

## 8.2 Zusammenfassung

Kalzium-abhängige Leitfähigkeiten werden als bedeutende Regulatoren des neuronalen Erregungsgeschehens angesehen. So wird beispielsweise angenommen, dass Ionenströme durch unspezifische Kationenkanäle ($I_{CAN}$) eine exzessive Abfolge von Aktionspotentialen („Bursts") auslösen, während Ionenströme durch $Ca^{2+}$-abhängige Kaliumkanäle ($I_{K,Ca}$) eine ruhigere Abfolge von Aktionspotentialen („tonisches" Feuerverhalten) der Nervenzelle bewirken. Die Kopplung von Kalziumeinstrom durch L-Typ spannungsgesteuerte Kalziumkanäle (LTCCs) an diese $Ca^{2+}$-abhängigen Leitfähigkeiten äußert sich elektrophysiologisch in Form von sogenannten Nachpotentialen. Das heißt depolarisiert man ein Neuron durch Strominjektion, kehrt das Membranpotential, nach Abschalten des Injektionsstromes, nicht umgehend zum Ausgangswert zurück, sondern es bilden sich Nachdepolarisationen (ADPs) oder Nachhyperpolarisationen (AHPs). Diese äußern sich am deutlichsten, wenn Aktionspotentiale durch das Kugelfischgift Tetrodotoxin (TTX), einem Blocker spannungsgesteuerter $Na^{+}$-Kanäle, unterbunden werden. In einer vorausgehenden Studie unserer Arbeitsgruppe an hippokampalen Neuronen von Ratten konnte auf diese Weise gezeigt werden, dass ADPs die CAN-Kopplung (exzitatorische Kopplung), und AHPs die $K_{CA}$-Kopplung (inhibitorische Kopplung) zugrunde liegt. Das Ziel meiner Studie war es demnach diese funktionellen Zusammenhänge, durch Bestimmung der bevorzugten LTCC-Kopplung und Registrierung des dominierenden Feuerverhaltens eines Neurons in Anwesenheit des LTCC-Aktivators BayK, im Detail zu untersuchen.

Dazu wurde die elektrische Aktivität einer Nervenzelle unter Applikation von BayK mittels der Stromklemme („current clamp") Technik aufgezeichnet. Anschließend wurde die Größe einzelner Burst-Entladungen, Aktionspotentiale und exzitatorischer (EPSPs) sowie inhibitorischer postsynaptischer Potentiale (IPSPs) bestimmt. Die bevorzugte LTCC-Kopplung in diesem Neuron wurde dann durch strominduzierte Depolarisationen in Anwesenheit von TTX identifiziert. Zusätzlich wurde die Aktivität von LTCCs durch Verwendung von BayK und dem LTCC Blocker Isradipin moduliert.

Meine Daten zeigen, dass die Entstehung von Bursts oder tonischem Feuerverhalten nicht von LTCC-CAN oder LTCC-KCa Kopplung abhängig ist, da beide Entladungsmuster in ADP- und AHP-erzeugenden Neuronen entdeckten werden konnten. Vielmehr scheint die Induktion eines dieser Feuerverhalten vom Membranpotential einer Zelle abzuhängen, da Bursts bevorzugt in Zellen mit hyperpolarisierten Membranpo-

tential ausgelöst wurde, während ein stärker depolarisiertes Membranpotential tonisches Feuerverhalten bewirkte. Weiters wurde die LTCC-CAN Kopplung durch kürze und schwächere Depolarisation induziert und könnte somit eine Rolle in der Entstehung von Bursts und/ oder der Plateauphase von Bursts spielen, wohingegen LTCC-$K_{Ca}$ Kopplung exponentiell mit länger andauernder Strominjektion zunahm und deshalb in die Beendigung von Bursts involviert sein könnte. Tatsächlich waren Bursts in ADP-erzeugenden Neuronen größer als in jenen Zellen, die ein AHP zeigten. Im Gegensatz dazu, konnten keine Unterschiede in der Größe von Aktionspotentialen, EPSPs und IPSPs zwischen den zwei experimentellen Gruppen detektiert werden. Zudem hatte das Ausmaß von ADPs oder AHPs keinen Einfluss auf die Größe von Bursts oder Aktionspotentialen in meinen Aufzeichnungen. Zusammengefasst deuten meine Daten darauf hin, dass LTCC-induzierte CAN und $K_{Ca}$ Aktivierung keine entscheidende, sondern eher eine modulatorische Rolle im hippokampalen Feuerverhalten spielen.

## 8.3 Acknowledgements

First of all, I want to thank Helmut Kubista for giving me the opportunity of working at this project and for always having time for my problems and questions.
Besides that I want to thank Axel Schmid for supervising this master thesis.
I am grateful to Stefan Böhm for being able to work in his lab.
Furthermore, I want to thank all the people in the lab, especially Gabi Gaupmann, for valuable advice and help.
Finally, I want to thank my family and my girlfriend for their support and motivation.

## 8.4 Curriculum vitae

### Education

| | |
|---|---|
| 2011 – 2014 | Master study Molecular Biology, University of Vienna |
| 2007 – 2011 | Bachelor study Biomedicine and Biotechnology, University of Veterinary Medicine Vienna |
| 2004 – 2007 | Academy of Orthoptics, General Hospital of Vienna |
| 1995 – 2003 | Secondary School Parhamerplatz 18, 1170 Vienna |
| 1991 – 1995 | Elementary School Halirschgasse 25, 1170 Vienna |

### Practical Experience

| | |
|---|---|
| 2012 – 2014 | Master thesis at the Department of Neurophysiology and Neuropharmacology, Center for Pharmacology and Physiology, Medical University of Vienna |
| 2012 | Practice at the Department of Neurophysiology and Neuropharmacology, Medical University of Vienna |
| 2011 | Bachelor thesis at the Department of Clinical Pharmacology, Section Ophthalmo-Pharmacology, Medical University of Vienna |
| 2010 | Practice at the Institute for Bacteriology, Mycology and Hygiene, University of Veterinary Medicine Vienna |
| 2009 | Practice at the Institute of Immunology, University of Veterinary Medicine Vienna |
| 2008 | Practice at the Institute of Laboratory Animal Science, University of Veterinary Medicine Vienna |
| 2007 | Practice at the Institute of Laboratory Animal Science, University of Veterinary Medicine Vienna |

### Skills

| | |
|---|---|
| Scientific skills | PCR, qPCR, RT-PCR, cell culture (embryonic stem cells, HeLa cells, mycoplasma, neurons), transfections, gel electrophoresis, vector cloning, restriction digest, ELISA, cell counting, flow cytometry (FCM), immunoprecipitation, SDS-PAGE, Western blot, Gentamicin-resistance assay, thin layer chromatography, photometric measurements, Patch Clamp measurements (current clamp mode), etc. |
| Language skills | English fluent in spoken and written, basics in French |
| Computer skills | MS-Office, Statistica, GraphPad Prism, SPSS, R, pClamp |

## Other activities

| | |
|---|---|
| 2013 | Congress attendance and poster presentation at the 19th Scientific Symposium of the Austrian Pharmacological Society (APHAR) and 13th Meeting of the Austrian Neuroscience Association (ANA) |

## Publication

Boltz A, **Ruiß M**, Jonas JB, Tao Y, Rensch F, Weger M, Garhöfer G, Frantal S, El-Shabrawi Y, Schmetterer L (2012) Role of vascular endothelial growth factor polymorphisms in the treatment success in patients with wet age-related macular degeneration. Ophthalmology 119(8):1615-20.